



Sliding Windows and Persistence: An Application of Topological Methods to Signal Analysis

Jose A. Perea · John Harer

Received: 12 March 2013 / Revised: 22 November 2013 / Accepted: 13 April 2014 /
Published online: 29 May 2014
© SFoCM 2014

Abstract We develop in this paper a theoretical framework for the topological study of time series data. Broadly speaking, we describe geometrical and topological properties of sliding window embeddings, as seen through the lens of persistent homology. In particular, we show that maximum persistence at the point-cloud level can be used to quantify periodicity at the signal level, prove structural and convergence theorems for the resulting persistence diagrams, and derive estimates for their dependency on window size and embedding dimension. We apply this methodology to quantifying periodicity in synthetic data sets and compare the results with those obtained using state-of-the-art methods in gene expression analysis. We call this new method **SW1PerS**, which stands for Sliding Windows and 1-Dimensional Persistence Scoring.

Keywords Persistent homology · Time-delay embeddings · Periodicity

Mathematics Subject Classification Primary 55U99 · 37M10 · 68W05 · Secondary 57M99

1 Introduction

Signal analysis is an enormous field. There are many methods to study signals and many applications of that study. Given its importance, one might conclude that there

Communicated by Herbert Edelsbrunner.

J. A. Perea (✉)

Department of Mathematics, Duke University, Durham, NC, USA
e-mail: joperea@math.duke.edu

J. Harer

Departments of Mathematics, Computer Science, and Electrical and Computer Engineering,
Duke University, Durham, NC, USA
e-mail: john.harer@duke.edu

is little opportunity left for the development of totally new approaches to signals. Yet in this paper we provide a new way to find periodicity and quasiperiodicity in signals. The method is based on sliding windows (also known as time-delay reconstruction), which have been used extensively in both engineering applications and in dynamical systems. But the approach presented here adds a new element not applied before, which comes from the new field of computational topology [12].

Persistent homology is a topological method for measuring the shapes of spaces and the features of functions. One of the most important applications of persistent homology is to point clouds [3], where shape is usually interpreted as the geometry of some implicit underlying object near which the point cloud is sampled. The simplest nontrivial example of this idea is a point cloud that has the shape of a circle, and this shape is captured with one-dimensional (1D) persistence. The challenge in applying the method is that noise can reduce the persistence, and not enough points can prevent the circular shape from appearing. It is also a challenge to deal with the fact that features come on all scale levels and can be nested or in more complicated relationships. But this is what persistent homology is all about.

The idea of applying 1D persistence to study time series arose in our study of gene expression data [11, 23]. The first of these papers studied a variety of existing methods for finding periodicity in gene expression patterns. The motivation of that work was the search for gene regulatory networks (more precisely, possible nodes of gene regulatory networks) that control periodic processes in cells such as the cell division cycle, circadian rhythms, metabolic cycles, and periodic patterning in biological development (lateral roots and somites). The methods studied in [11] were derived from a number of fields, including astronomy, geometry, biology, and statistics, and all were based on a direct study of the underlying signal in either physical or frequency space. The most successful methods are based on finding cosinelike behavior, a rather limited definition of periodicity.

In this paper and in [23] we look instead at the shape of the sliding window point cloud, a totally different approach. Of course, the geometry of point clouds derived from other kinds of data like images has been studied [4, 16], but the current approach is quite different. Our method understands periodicity as the repetition of patterns, whatever these may be, and quantifies this recurrence as the degree of circularity/roundness in the generated point-cloud. Thus, it is fundamentally agnostic.

1.1 Previous Work

The sliding window, or time-delay embedding, has been used mostly in the study of dynamical systems to understand the nature of their attractors. Takens' theorem [28] gives conditions under which a smooth attractor can be reconstructed from the observations of a function, with bounds related to those of the Whitney embedding theorem. This methodology has in turn been employed to test for nonlinearity and chaotic behavior in the dynamics of Electroencephalogram, Electrocardiogram, and Electromyogram [25, 26].

It was recently demonstrated by [10] that combining time-delay embeddings with topological methods provides a framework for parameterizing periodic systems.

[16] provide in their Chap. 1 a good source of examples of time-delay embeddings used in real-world data sets.

1.2 Our Contribution

In the aforementioned applications, little of the topology and none of the geometry of the resulting sliding window embedding have ever been used. The novelty of our approach lies in our use of this geometry and topology through persistent homology. We make this possible by showing that maximum persistence, as a measure of the *roundness* of the point cloud, occurs when the window size corresponds to the natural frequency of the signal. This means that 1D persistence is an effective quantifier of periodicity and quasiperiodicity and can be used to infer properties of the signal.

1.3 Outline

In Sect. 2 we show a motivating example to illustrate our perspective. In Sect. 3 we give a general introduction to persistent homology. More on this topic can be found in [12]. In Sect. 4 we show that sliding windows behave well under approximations, and we give explicit estimates at the point-cloud level. Section 5 is devoted to studying the geometric structure of sliding-window embeddings from truncated Fourier series and their dependency on embedding dimension and window size. In Sect. 6 we prove results describing the structure of persistent diagrams from sliding-window embeddings. Some examples of how our method applies in the problem of quantifying periodicity in time series data are given in Sect. 7.

2 Definitions and Motivation

Suppose that f is a function defined on an interval of the real numbers. Choose an integer M and a real number τ , both greater than 0. The sliding-window embedding of f based at $t \in \mathbb{R}$ into \mathbb{R}^{M+1} is the point

$$SW_{M,\tau} f(t) = \begin{bmatrix} f(t) \\ f(t + \tau) \\ \vdots \\ f(t + M\tau) \end{bmatrix}.$$

Choosing different values of t gives a collection of points called a **sliding-window point cloud for f** . A critical parameter for this embedding is the **window size $M\tau$** .

2.1 Motivation

To motivate the approach we take in the paper, let us begin with the following example.

Example. Let $L \in \mathbb{N}$ and $f(t) = \cos(Lt)$. Then

$$\begin{aligned}
SW_{M,\tau}f(t) &= \begin{bmatrix} \cos(Lt) \\ \cos(Lt + L\tau) \\ \vdots \\ \cos(Lt + LM\tau) \end{bmatrix} \\
&= \cos(Lt) \begin{bmatrix} 1 \\ \cos(L\tau) \\ \vdots \\ \cos(LM\tau) \end{bmatrix} - \sin(Lt) \begin{bmatrix} 0 \\ \sin(L\tau) \\ \vdots \\ \sin(LM\tau) \end{bmatrix} \\
&= \cos(Lt)\mathbf{u} - \sin(Lt)\mathbf{v},
\end{aligned}$$

and therefore $t \mapsto SW_{M,\tau}f(t)$ describes a planar curve in \mathbb{R}^{M+1} , with winding number L , whenever \mathbf{u} and \mathbf{v} are linearly independent. One can in fact see how the shape of this curve changes as a function of L , M , and τ . Indeed, let

$$A = \begin{bmatrix} \|\mathbf{u}\|^2 & -\langle \mathbf{u}, \mathbf{v} \rangle \\ -\langle \mathbf{u}, \mathbf{v} \rangle & \|\mathbf{v}\|^2 \end{bmatrix},$$

which can be computed using Lagrange's trigonometric formulae

$$\begin{aligned}
\langle \mathbf{u}, \mathbf{v} \rangle &= \frac{1}{2} \sum_{m=0}^M \sin(2Lm\tau) = \frac{\sin(L(M+1)\tau) \sin(LM\tau)}{2 \sin(L\tau)} \\
\|\mathbf{u}\|^2 - \|\mathbf{v}\|^2 &= \sum_{m=0}^M \cos(2Lm\tau) = \frac{\sin(L(M+1)\tau) \cos(LM\tau)}{\sin(L\tau)} \\
\|\mathbf{u}\|^2 + \|\mathbf{v}\|^2 &= M+1.
\end{aligned}$$

It follows that A is positive semidefinite (both its determinant and trace are nonnegative). This means the eigenvalues of A are nonnegative and real, $\lambda_1 \geq \lambda_2 \geq 0$, and there is a 2×2 orthogonal matrix B such that

$$A = B^T \Lambda^2 B, \quad \text{where} \quad \Lambda = \begin{bmatrix} \sqrt{\lambda_1} & 0 \\ 0 & \sqrt{\lambda_2} \end{bmatrix}.$$

Therefore, if $\mathbf{x}(t) = [\cos(Lt) \ \sin(Lt)]'$ (here $'$ denotes transpose), then

$$\begin{aligned}
\|SW_{M,\tau}f(t)\|^2 &= \left\| \begin{bmatrix} 1 & 1 \\ \mathbf{u} & -\mathbf{v} \\ 1 & 1 \end{bmatrix} \mathbf{x}(t) \right\|^2 \\
&= \langle \mathbf{x}(t), A \mathbf{x}(t) \rangle \\
&= \langle \Lambda B \mathbf{x}(t), \Lambda B \mathbf{x}(t) \rangle.
\end{aligned}$$

Since B is a rotation matrix, say by an angle α , then the map

$$SW_{M,\tau} f(t) \mapsto \begin{bmatrix} \sqrt{\lambda_1} \cos(Lt + \alpha) \\ \sqrt{\lambda_2} \sin(Lt + \alpha) \end{bmatrix}$$

is an isometry.

In summary, for $f(t) = \cos(Lt)$, the embedding $t \mapsto SW_{M,\tau} f(t)$ describes an ellipse on the plane $\text{Span}\{\mathbf{u}, \mathbf{v}\}$ whose shape (minor and major axes) is determined by the square roots of the eigenvalues of A . These eigenvalues can be computed explicitly as

$$\lambda_1 = \frac{(M+1) + \left| \frac{\sin(L(M+1)\tau)}{\sin(L\tau)} \right|}{2},$$

$$\lambda_2 = \frac{(M+1) - \left| \frac{\sin(L(M+1)\tau)}{\sin(L\tau)} \right|}{2}.$$

It follows that the ellipse is roundest when λ_2 attains its maximum, which occurs if and only if $L(M+1)\tau \equiv 0 \pmod{\pi}$. One such instance is

$$M\tau = \left(\frac{M}{M+1} \right) \frac{2\pi}{L},$$

which is when the window-size approximates the length of the period of $f(t)$. In other words, the roundness of the sliding-window point cloud for $f(t) = \cos(Lt)$ is maximized when the window size is close to resonating with its natural frequency.

The previous example provides the following intuition: for a generic function f , the degree to which the image of $SW_{M,\tau} f$ traces a closed curve in \mathbb{R}^{M+1} reflects how periodic f is. Moreover, if f is periodic, then the roundness of $SW_{M,\tau} f$ defined as the largest radius of a ball in \mathbb{R}^{M+1} so that the curve

$$t \mapsto SW_{M,\tau} f(t)$$

is tangent to at least two points of its equator is maximized when the window size $M\tau$ approaches the period length. The goal of this paper is to understand these relations.

The geometry of the curve $t \mapsto SW_{M,\tau} f(t)$ can be quite complicated, as shown in Fig. 1. The 1D persistence diagram for the Vietoris–Rips filtration on a finite sample $\{SW_{M,\tau} f(t_1), \dots, SW_{M,\tau} f(t_S)\}$, on the other hand, is readily computable [29,30], and its maximum persistence is a measure of roundness as defined in the previous paragraph. We will review in Sect. 3 the basic concepts behind persistent homology and devote the rest of the paper to understanding how the geometry of $SW_{M,\tau} f$ reflects properties of f such as periodicity and period.

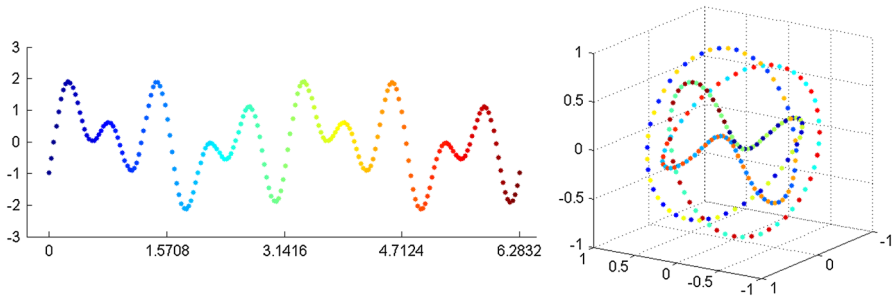


Fig. 1 From a periodic function to its sliding-window point cloud. *Left*: periodic function f . *Right*: multidimensional scaling into \mathbb{R}^3 for $SW_{20,\tau} f$. For each t we use the same color for $f(t)$ and $SW_{20,\tau} f(t)$. Please refer to the electronic colored version

2.2 Approach

With this motivation in mind, we now describe our approach: as we have seen, understanding the algebraic properties of trigonometric functions allows one to characterize the geometry of $SW_{M,\tau} f$ when f is a trigonometric polynomial. This understanding, in turn, can be bootstrapped using Fourier analysis and the stability of persistence diagrams in an approximation step toward $SW_{M,\tau}$ of a generic periodic function. In what follows, we will establish the appropriate continuity results for approximation and the necessary structural results for persistence diagrams from sliding-window point clouds.

3 Background: Persistent Homology

In this section we define the key concepts that underlie the theory of persistent homology for filtered simplicial complexes. We give a terse introduction to simplicial homology, but more information can be found in [14] and [21].

3.1 Homology of Simplicial Complexes

Let K be a simplicial complex and p a prime number. Recall that this means that K is a finite set of simplices that is closed under the face relation and that two simplices of K are either disjoint or intersect in a common face. Let \mathbb{F}_p be the finite field with p elements; the \mathbb{F}_p vector space generated by the k -dimensional simplices of K is denoted by $C_k(K)$. It consists of all k -chains, which are finite formal sums $c = \sum_j \gamma_j x_j$, with $\gamma_j \in \mathbb{F}_p$ and each x_j a k -simplex in K . The boundary $\partial(x_j)$ is the alternating formal sum of the $(k-1)$ -dimensional faces of x_j , and the boundary of the chain c is obtained by extending ∂ linearly:

$$\partial(c) = \sum_j \gamma_j \partial(x_j).$$

It is not difficult to check that $\partial \circ \partial = \partial^2 = 0$. The k -chains that have boundary 0 are called k -cycles; they form a subspace Z_k of C_k . The k -chains that are the boundary of $(k + 1)$ -chains are called k -boundaries and form a subspace B_k of C_k . The fact that $\partial^2 = 0$ tells us that $B_k \subset Z_k$. The quotient group $H_k(K) = Z_k/B_k$ is the k th simplicial homology group of K with \mathbb{F}_p -coefficients. The rank of $H_k(K)$ is the k th mod p Betti number of K and is denoted by $\beta_k(K)$. Since the prime p will be clear from the context, we do not include it in the notation.

When we have two simplicial complexes K and K' , a simplicial map $f : K \rightarrow K'$ is a continuous map that takes simplices to simplices and is linear on each. A simplicial map induces a homomorphism on homology, $f_* : H_k(K) \rightarrow H_k(K')$, and homotopic maps induce the same homomorphism. Homotopy equivalences of spaces induce isomorphisms on homology. The simplicial approximation theorem tells us that a continuous map of simplicial complexes can be approximated by a simplicial map, so that it makes sense to talk about continuous maps inducing homomorphisms on homology.

3.1.1 Persistence

We next define persistence, persistent homology, and the persistence diagram for a simplicial complex K . A subcomplex of K is a subset of its simplices that is closed under the face relation. A filtration of K is a nested sequence of subcomplexes that starts with an empty complex and ends with a complete complex,

$$\emptyset = K_0 \subset K_1 \subset \cdots \subset K_m = K.$$

A homology class α is born at K_i if it is not in the image of the map induced by the inclusion $K_{i-1} \subset K_i$. If α is born at K_i , then we say that it dies entering K_j if the image of the map induced by $K_{i-1} \subset K_{j-1}$ does not contain the image of α but the image of the map induced by $K_{i-1} \subset K_j$ does. The persistence of α is $j - i$.

We code birth and death information in persistence diagrams, one for each dimension. The diagram $\text{dgm}(k)$ has a point (i, j) for every k -homology class that is born at K_i and dies entering K_j . For most of the paper the homological dimension k will be clear from the context or unimportant for the discussion. To ease notation, we will simply write dgm instead of $\text{dgm}(k)$ and let dgm_1 and dgm_2 denote two k -persistence diagrams to be compared. Sometimes we have a function h that assigns a height or distance to each subcomplex K_i , and in that case we use the pair $(h(i), h(j))$. Each diagram is now a multiset since classes can be born simultaneously and die simultaneously. We adjoin the diagonal $\Delta = \{(x, x) : x \geq 0\}$ to each diagram and endow each point $(x, x) \in \Delta$ with countable multiplicity.

The bottleneck distance between two persistence diagrams dgm_1 and dgm_2 is defined by

$$d_B(\text{dgm}_1, \text{dgm}_2) = \inf_{\phi} \sup_{x \in \text{dgm}_1} \|x - \phi(x)\|_{\infty},$$

where the infimum is taken over all bijections $\phi : \text{dgm}_1 \rightarrow \text{dgm}_2$. Note that such ϕ exist even if the number of points of dgm_1 and dgm_2 are different since we have included the diagonal.

3.1.2 Rips Complex

Let $X \subset \mathbb{R}^n$ be a compact set, for example, a finite point cloud. We define $d_X(y)$ as the distance from the point $y \in \mathbb{R}^n$ to X . We are interested in how the homology of the sublevel sets $X_r = d_X^{-1}([0, r])$ changes as we increase r . To make this computationally feasible, we replace the continuous family of spaces X_r with a discrete family of approximations called the Rips complexes defined as follows. Fix $r \geq 0$; $R_r(X)$ is the simplicial complex whose vertices are the points of X and whose k -simplices are the $k + 1$ tuples $[x_0, \dots, x_k]$ such that the pairwise distances $\|x_i - x_j\|$ are less than or equal to r for all $0 \leq i < j \leq k$. Note that the edges determine the simplices of $R_r(X)$, that a higher-dimensional simplex is added if and only if all its edges have been added, and that the Rips construction makes sense for any metric space.

Since $R_r(X) \subset R_s(X)$ whenever $r < s$, the Rips complexes form a filtration of R_∞ , which denotes the largest simplicial complex having X as its vertex set. Changes occur at the finite set of r values that are pairwise distances between points, so we can work with just these r_j to get the filtration

$$X = R_0 \subset R_1 \subset \dots \subset R_m,$$

where $R_j = R_{r_j}(X)$ and $R_m = R_\infty$. We will use this filtered complex to study the persistence and the persistence diagrams of the point cloud X . We thus denote by $\text{dgm}(X)$ the persistence diagram of the homology filtration induced from the Rips filtration on X , where we use homology with coefficients in \mathbb{F}_p .

A key property of persistence is that it is *stable* [6]. In our context this means that if X, Y are two point clouds and d_H, d_{GH} are the Hausdorff and Gromov–Hausdorff distances, then

$$d_B(\text{dgm}(X), \text{dgm}(Y)) \leq 2d_{GH}(X, Y) \leq 2d_H(X, Y). \quad (1)$$

4 Approximation Theorem

In this section we show that one can study $SW_{M,\tau}f$ and the persistence of the point cloud it generates for a generic function $f \in L^2(\mathbb{T} = \mathbb{R}/2\pi\mathbb{Z})$ by using its Fourier series approximation. While it seems quite difficult to study $SW_{M,\tau}f$ directly, it is not hard to understand $SW_{M,\tau} \cos(nt)$ and $SW_{M,\tau} \sin(nt)$, so we will build our understanding of the geometry of a general $SW_{M,\tau}f$ from these special cases using the Fourier series of f . To do this, we will need to show that $SW_{M,\tau}$ behaves well under approximations and that these approximations work in the context of stability for persistence diagrams.

Let $C(X, Y)$ denote the set of continuous functions from X to Y equipped with the sup norm. The sliding-window embedding induces a mapping

$$SW_{M,\tau} : C(\mathbb{T}, \mathbb{R}) \longrightarrow C(\mathbb{T}, \mathbb{R}^{M+1}).$$

The first fact about this map that we need is the following proposition.

Proposition 4.1 *Let $\mathbb{T} = \mathbb{R}/2\pi\mathbb{Z}$. Then for all $M \in \mathbb{N}$ and $\tau > 0$, the mapping $SW_{M,\tau} : C(\mathbb{T}, \mathbb{R}) \longrightarrow C(\mathbb{T}, \mathbb{R}^{M+1})$ is a bounded linear operator with norm $\|SW_{M,\tau}\| \leq \sqrt{M+1}$.*

Proof The linearity of $SW_{M,\tau}$ follows directly from its definition. To see that it is bounded, notice that for every $f \in C(\mathbb{T}, \mathbb{R})$ and $t \in \mathbb{T}$ we have

$$\begin{aligned} \|SW_{M,\tau} f(t)\|_{\mathbb{R}^{M+1}}^2 &= |f(t)|^2 + |f(t+\tau)|^2 + \cdots + |f(t+M\tau)|^2 \\ &\leq (M+1) \|f\|_{\infty}^2. \end{aligned}$$

□

We now consider approximating a function f by its Fourier polynomials and study how the sliding windows behave in this context. In particular, let

$$f(t) = S_N f(t) + R_N f(t),$$

where

$$S_N f(t) = \sum_{n=0}^N a_n \cos(nt) + b_n \sin(nt) = \sum_{n=-N}^N \widehat{f}(n) e^{int}$$

is the N -truncated Fourier series expansion of f , $R_N f$ is the remainder, and

$$\widehat{f}(n) = \begin{cases} \frac{1}{2}a_n - \frac{i}{2}b_n & \text{if } n > 0, \\ \frac{1}{2}a_{-n} + \frac{i}{2}b_{-n} & \text{if } n < 0, \\ a_0 & \text{if } n = 0. \end{cases} \quad (2)$$

We can easily compute that

$$SW_{M,\tau} f(t) = \sum_{n=0}^N \cos(nt) (a_n \mathbf{u}_n + b_n \mathbf{v}_n) + \sin(nt) (b_n \mathbf{u}_n - a_n \mathbf{v}_n) + SW_{M,\tau} R_N f(t),$$

where

$$\mathbf{u}_n = SW_{M,\tau} \cos(nt) \big|_{t=0} \quad \text{and} \quad \mathbf{v}_n = SW_{M,\tau} \sin(nt) \big|_{t=0}.$$

The vectors \mathbf{u}_n and \mathbf{v}_n form a fundamental basis out of which we can build our understanding of the structure of the point clouds that sliding windows create. We introduce the notation

$$\phi_\tau(t) = \sum_{n=0}^N \cos(nt)(a_n \mathbf{u}_n + b_n \mathbf{v}_n) + \sin(nt)(b_n \mathbf{u}_n - a_n \mathbf{v}_n)$$

for the sliding-window embedding for $S_N f(t)$. Also, when f , M , and N are clear from the context, we will simply write $\phi_\tau = SW_{M,\tau} S_N f$.

The next step is to find a bound on the term $SW_{M,\tau} R_N f(t)$. We will actually find a series of bounds, one for each of the derivatives $f^{(k)} = \frac{d^k f}{dt^k}$, whenever they exist and are continuous.

Proposition 4.2 *Let $k \in \mathbb{N}$. If $f \in C^k(\mathbb{T}, \mathbb{R})$, then for all $t \in \mathbb{T}$*

$$\|SW_{M,\tau} f(t) - \phi_\tau(t)\|_{\mathbb{R}^{M+1}} \leq \sqrt{4k-2} \|R_N f^{(k)}\|_2 \cdot \frac{\sqrt{M+1}}{(N+1)^{k-\frac{1}{2}}}.$$

Proof If $k \in \mathbb{N}$ and $f \in C^k(\mathbb{T}, \mathbb{R})$, then integration by parts yields the well-known identity

$$|\widehat{f^{(k)}}(n)| = |n|^k |\widehat{f}(n)|$$

for the length of $\widehat{f^{(k)}}(n)$, the n th complex Fourier coefficient of $f^{(k)}$, $n \in \mathbb{Z}$. Thus, for all $t \in \mathbb{T}$ the Cauchy–Schwartz inequality, Young’s inequality and Parseval’s theorem together imply that

$$\begin{aligned} |R_N f(t)| &\leq \sum_{n=N+1}^{\infty} \frac{|\widehat{f^{(k)}}(n)| + |\widehat{f^{(k)}}(-n)|}{n^k} \\ &\leq \left(\sum_{n=N+1}^{\infty} (|\widehat{f^{(k)}}(n)| + |\widehat{f^{(k)}}(-n)|)^2 \right)^{1/2} \cdot \left(\sum_{n=N+1}^{\infty} \frac{1}{n^{2k}} \right)^{1/2} \\ &\leq \left(2 \sum_{|n| \geq N+1} |\widehat{f^{(k)}}(n)|^2 \right)^{1/2} \cdot \left(\int_{N+1}^{\infty} \frac{1}{x^{2k}} dx \right)^{1/2} \\ &= \sqrt{2} \|R_N f^{(k)}\|_2 \cdot \frac{\sqrt{2k-1}}{(N+1)^{k-\frac{1}{2}}}, \end{aligned}$$

and hence, by Proposition 4.1,

$$\begin{aligned} \|SW_{M,\tau} f(t) - \phi_\tau(t)\|_{\mathbb{R}^{M+1}} &\leq \sqrt{M+1} \|R_N f\|_\infty \\ &\leq \sqrt{4k-2} \left\| R_N f^{(k)} \right\|_2 \cdot \frac{\sqrt{M+1}}{(N+1)^{k-\frac{1}{2}}}. \end{aligned}$$

□

These bounds readily imply estimates for the Hausdorff distance between the sliding-window point clouds of f and $S_N f$. Indeed, let X and Y be the images of $T \subset \mathbb{T}$ through $SW_{M,\tau} f$ and ϕ_τ , respectively. It follows that if $f \in C^k(\mathbb{T}, \mathbb{R})$ and

$$\epsilon > \sqrt{4k-2} \left\| R_N f^{(k)} \right\|_2 \frac{\sqrt{M+1}}{(N+1)^{k-\frac{1}{2}}},$$

then $X \subset Y^\epsilon$, $Y \subset X^\epsilon$, and, therefore, $d_H(X, Y) \leq \epsilon$. Letting ϵ approach its lower bound and using the stability of d_B with respect to d_H (Eq. 1), we obtain the relation

$$d_B(\text{dgm}(X), \text{dgm}(Y)) \leq 2\sqrt{4k-2} \left\| R_N f^{(k)} \right\|_2 \frac{\sqrt{M+1}}{(N+1)^{k-\frac{1}{2}}}.$$

As described in the introduction, the maximum persistence of $\text{dgm}(X)$ will serve to quantify the periodicity of f when measured with sliding windows of length $M\tau$. By the maximum persistence of a diagram dgm , we mean the following.

Definition 4.3 Let $(x, y) \in \text{dgm}$, and define $\text{pers}(x, y) = y - x$ for $(x, y) \in \mathbb{R}^2$, and as ∞ otherwise. We let

$$mp(\text{dgm}) = \max_{\mathbf{x} \in \text{dgm}} \text{pers}(\mathbf{x})$$

denote the maximum persistence of dgm .

Remark 4.4 If dgm_Δ denotes the diagram with the diagonal as underlying set, each point endowed with countable multiplicity, then

$$mp(\text{dgm}) = 2d_B(\text{dgm}, \text{dgm}_\Delta).$$

Indeed, for any bijection $\phi : \text{dgm} \rightarrow \text{dgm}_\Delta$ and every $\mathbf{x} \in \text{dgm}$

$$\|\mathbf{x} - \phi(\mathbf{x})\|_\infty \geq \frac{1}{2} \text{pers}(\mathbf{x})$$

with equality if and only if $\phi(x, y) = (\frac{x+y}{2}, \frac{x+y}{2})$. Thus,

$$\max_{\mathbf{x} \in \text{dgm}} \|\mathbf{x} - \phi(\mathbf{x})\| \geq \frac{1}{2} mp(\text{dgm}),$$

and therefore $d_B(\text{dgm}, \text{dgm}_\Delta) = \min_{\phi} \max_{\mathbf{x} \in \text{dgm}} \|\mathbf{x} - \phi(\mathbf{x})\| \geq \frac{1}{2} mp(\text{dgm})$. For the reverse inequality, notice that the map

$$(x, y) \mapsto \left(\frac{x+y}{2}, \frac{x+y}{2} \right)$$

extends to a bijection $\phi_0 : \text{dgm} \rightarrow \text{dgm}_\Delta$ of multisets such that for all $\mathbf{x} \in \text{dgm}$ one has $\|\mathbf{x} - \phi_0(\mathbf{x})\|_\infty = \frac{1}{2} \text{pers}(\mathbf{x})$.

We summarize the results of this section in the following theorem.

Theorem 4.5 (Approximation) *Let $T \subset \mathbb{T}$, $f \in C^k(\mathbb{T}, \mathbb{R})$, $X = SW_{M,\tau} f(T)$, and $Y = SW_{M,\tau} S_N f(T)$. Then*

(1)

$$d_H(X, Y) \leq \sqrt{4k-2} \left\| R_N f^{(k)} \right\|_2 \frac{\sqrt{M+1}}{(N+1)^{k-\frac{1}{2}}},$$

(2)

$$|mp(\text{dgm}(X)) - mp(\text{dgm}(Y))| \leq 2d_B(\text{dgm}(X), \text{dgm}(Y)),$$

(3)

$$d_B(\text{dgm}(X), \text{dgm}(Y)) \leq 2\sqrt{4k-2} \left\| R_N f^{(k)} \right\|_2 \frac{\sqrt{M+1}}{(N+1)^{k-\frac{1}{2}}}.$$

It follows that the persistent homology of the sliding-window point cloud of a function $f \in C^k(\mathbb{T}, \mathbb{R})$ can, in the limit, be understood in terms of that of its truncated Fourier series.

Remark 4.6 Regarding the hypothesis of f being at least C^1 , Proposition 4.2 (which is the basis of the approximation theorem, Theorem 4.5) only uses that $f' \in L^2(\mathbb{T})$; thus, everything up to this point (and, in fact, for the rest of the paper) holds true for functions in the Sobolev space $W^{1,2}(\mathbb{T})$. The reason why we have phrased the results in terms of the spaces $C^k(\mathbb{T})$ is because it provides the following interpretation: if the function f has a certain degree of niceness, then one should expect the approximation of the persistence diagrams from $SW_{M,\tau} f$ by those of $SW_{M,\tau} S_N f$ to improve at an explicit rate. Moreover, the nicer the function, the better the rate.

Another function space for which our arguments apply is the set of Hölder-continuous functions with exponent $\alpha \in (\frac{1}{2}, 1)$. Indeed, if for such an f one considers the Fejér approximation

$$\sigma_N f(t) = \sum_{|n| \leq N} \left(1 - \frac{|n|}{N+1} \right) \cdot \widehat{f}(n) e^{int}$$

then [see Theorem 1.5.3 in [22]]

$$\|\sigma_N f - f\|_\infty \leq \frac{C_\alpha K_\alpha}{N^\alpha},$$

where K_α is the Hölder constant of f and C_α is a constant depending solely on α . Hence, one obtains the following version of Proposition 4.2: for every $t \in \mathbb{T}$

$$\|SW_{M,\tau} f(t) - SW_{M,\tau} \sigma_N f(t)\|_{\mathbb{R}^{M+1}} \leq C_\alpha K_\alpha \frac{\sqrt{M+1}}{N^\alpha}$$

and the corresponding version of the approximation theorem follows. Later on (e.g., in Theorem 6.8) we will use some bounds in terms of $\|f'\|_2$ and $\|S_N f'\|_2$. Adapting the results involving such bounds to the Hölder-continuous setting requires some work: one can use the fact that every Hölder function has a Lipschitz approximation and then invoke Rademacher's theorem. We leave the details to the interested reader.

5 Geometric Structure of $SW_{M,\tau} S_N f$

We now turn our attention to the sliding-window construction applied to the truncated Fourier series of a periodic function. More specifically, we study the geometric structure of the sliding-window point cloud and its dependency on τ , N , and M .

Our focus on geometry contrasts with the methods used by others to determine τ and M . Traditionally, $M\tau$, the window size, is estimated using the autocorrelation function [17], while M is sometimes estimated directly using the method of false nearest neighbors [16].

5.1 Dimension of Embedding

One way of interpreting the embedding dimension, $M + 1$, is as the level of detail (from the function) one hopes to capture with the sliding-window representation. Given the advantages of a description that is as detailed as possible, it can be argued that large dimensions are desirable. From a computational perspective, however, this is a delicate point as our ultimate goal is to compute the persistent homology of the associated sliding-window point cloud. Indeed, as the dimension of the embedding grows, it follows that the point cloud needs to be (potentially) more densely populated. This causes the size of the Rips complex to outweigh the computational resources, making the persistent homology calculation unfeasible.

While there has been considerable progress on dealing with the size problem of the Rips complex [20], it is important to have a sense of the amount of retained information given the computational constraints on the embedding dimension. Fortunately, when dealing with trigonometric polynomials, the answer is clear: one loses no information if and only if the embedding dimension is greater than twice the maximum frequency. Indeed, recall the linear decomposition

$$SW_{M,\tau} S_N f(t) = \sum_{n=0}^N \cos(nt) (a_n \mathbf{u}_n + b_n \mathbf{v}_n) + \sin(nt) (b_n \mathbf{u}_n - a_n \mathbf{v}_n),$$

where

$$\mathbf{u}_n = SW_{M,\tau} \cos(nt) \Big|_{t=0}, \quad \mathbf{v}_n = SW_{M,\tau} \sin(nt) \Big|_{t=0}$$

and a_n, b_n are as defined in Eq. 2. Since the angles between the \mathbf{u}_n and the \mathbf{v}_m , as well as their norms, can be determined from M and τ (see example in Sect. 2.1), $S_N f$ can be recovered from $SW_{M,\tau} S_N f$ if the \mathbf{u}_n and the \mathbf{v}_m are linearly independent. This is the sense in which we say that there is no loss of information.

Proposition 5.1 *Let $M\tau < 2\pi$. Then $\mathbf{u}_0, \mathbf{u}_1, \mathbf{v}_1, \dots, \mathbf{u}_N, \mathbf{v}_N$ are linearly independent if and only if $M \geq 2N$.*

Proof If $2N + 1$ vectors in \mathbb{R}^{M+1} are linearly independent, it readily follows that $2N \leq M$. Let us assume now that $\mathbf{u}_0, \mathbf{u}_1, \mathbf{v}_1, \dots, \mathbf{u}_N, \mathbf{v}_N$ are linearly dependent, and let us show that $2N > M$ or, equivalently, that $2N \geq M + 1$. Indeed, let $\gamma_0, \beta_0, \dots, \gamma_N, \beta_N \in \mathbb{R}$ be scalars not all zero (set $\beta_0 = 0$), so that

$$\gamma_0 \mathbf{u}_0 + \beta_0 \mathbf{v}_0 + \dots + \gamma_N \mathbf{u}_N + \beta_N \mathbf{v}_N = \mathbf{0}.$$

That is, for all $m = 0, \dots, M$ we have

$$0 = \sum_{n=0}^N \gamma_n \cos(nm\tau) + \beta_n \sin(nm\tau) = \operatorname{Re} \left(\sum_{n=0}^N (\gamma_n - i\beta_n) e^{inm\tau} \right).$$

Let $\xi_m = e^{im\tau}$, $p(z) = \sum_{n=0}^N (\gamma_n + i\beta_n) z^n$, $\bar{p}(z) = \sum_{n=0}^N (\gamma_n - i\beta_n) z^n$, and

$$q(z) = z^N \cdot \left(\bar{p}(z) + p\left(\frac{1}{z}\right) \right).$$

It follows that $q(z)$ is a nonconstant complex polynomial of degree at most $2N$ and that for $m = 0, \dots, M$ we have $0 = \operatorname{Re}(\bar{p}(\xi_m))$. This implies that

$$\begin{aligned} q(\xi_m) &= (\xi_m)^N \left(\bar{p}(\xi_m) + p\left(\frac{1}{\xi_m}\right) \right) \\ &= (\xi_m)^N \left(\bar{p}(\xi_m) + p(\bar{\xi}_m) \right) \\ &= 2(\xi_m)^N \operatorname{Re}(\bar{p}(\xi_m)) \\ &= 0, \end{aligned}$$

and therefore ξ_0, \dots, ξ_M are roots of $q(z)$. Since $M\tau < 2\pi$, then $\xi_0, \xi_1, \dots, \xi_M$ are distinct, and we have that

$$M + 1 \leq \deg(q(z)) \leq 2N.$$

□

It is useful to contrast Proposition 5.1 with two important results in signal analysis: Takens' theorem from dynamical systems [28] and the Nyquist–Shannon sampling theorem from information theory [27]. Takens' theorem gives sufficient conditions on the length of a sequence of observation, so that the resulting embedding recovers the topology of a smooth attractor in a chaotic dynamical system. The aforementioned condition is that the dimension of the embedding should be greater than twice (an appropriate notion of) that of the attractor. The Nyquist–Shannon sampling theorem, on the other hand, contends that a band-limited signal can be recovered (exactly) from a sequence of observations whenever the sampling frequency is greater than twice the position, in the frequency domain, of the limiting band. The conclusion: in the case of trigonometric polynomials and the sliding-window construction, the usual sufficient condition on the dimension of the embedding and maximum frequency is also necessary.

Important assumption unless otherwise stated, given $N \in \mathbb{N}$, we will always set $M = 2N$ and require $\tau > 0$ to be such that $M\tau < 2\pi$.

5.2 Window Size and Underlying Frequency

As we saw in Sect. 2 on definitions and motivation, the sliding window point cloud for $\cos(Lt)$ describes a planar ellipse that is roundest when $\|\mathbf{u}\| - \|\mathbf{v}\| = \langle \mathbf{u}, \mathbf{v} \rangle = 0$ or, equivalently, when

$$L(M+1)\tau \equiv 0 \pmod{\pi}.$$

This uncovers a fundamental relation between window size, 1D persistence, and underlying frequency: the maximum persistence of the sliding-window point cloud from $\cos(Lt)$ is largest when the window size $M\tau$ is proportional to the underlying frequency $\frac{2\pi}{L}$, with proportionality constant $\frac{M}{M+1}$.

For the case of the truncated Fourier series $S_N f$ from a periodic function f , we will see shortly that if the same proportionality relation between window size and underlying frequency holds, then

$$SW_{M,\tau} S_N f(t) = \sum_{n=0}^N \cos(nt) (a_n \mathbf{u}_n + b_n \mathbf{v}_n) + \sin(nt) (b_n \mathbf{u}_n - a_n \mathbf{v}_n) \quad (3)$$

is a linear decomposition into mutually orthogonal vectors. We begin with the now familiar case of the restriction to $\text{Span}\{\mathbf{u}_n, \mathbf{v}_n\}$.

Proposition 5.2 For $n \geq 1$, $\langle \mathbf{u}_n, \mathbf{v}_n \rangle = \|\mathbf{u}_n\|^2 - \|\mathbf{v}_n\|^2 = 0$ if and only if

$$n(M+1)\tau \equiv 0 \pmod{\pi}.$$

Proof

$$\begin{aligned}
 \langle \mathbf{u}_n, \mathbf{v}_n \rangle &= \sum_{m=1}^M \cos(nm\tau) \sin(nm\tau) = \frac{1}{2} \sum_{m=1}^M \sin(2nm\tau) \\
 &= \frac{1}{2} \operatorname{Im} \left(\sum_{m=1}^M z_{2n\tau}^m \right), \quad \text{where } z_\theta = e^{i\theta} \\
 &= \frac{1}{2} \operatorname{Im} \left(\frac{1 - z_{2n(M+1)\tau}}{1 - z_{2n\tau}} - 1 \right) \\
 &= \frac{1}{2} \operatorname{Im} \left(\frac{1 - z_{2n(M+1)\tau}}{1 - z_{2n\tau}} \right) \\
 \|\mathbf{u}_n\|^2 - \|\mathbf{v}_n\|^2 &= \sum_{m=0}^M \cos^2(nm\tau) - \sin^2(nm\tau) \\
 &= \operatorname{Re} \left(\frac{1 - z_{2n(M+1)\tau}}{1 - z_{2n\tau}} \right),
 \end{aligned}$$

and therefore

$$4\langle \mathbf{u}_n, \mathbf{v}_n \rangle^2 + (\|\mathbf{u}_n\|^2 - \|\mathbf{v}_n\|^2)^2 = \left\| \frac{1 - z_{2n(M+1)\tau}}{1 - z_{2n\tau}} \right\|^2.$$

It follows that $\langle \mathbf{u}_n, \mathbf{v}_n \rangle = \|\mathbf{u}_n\|^2 - \|\mathbf{v}_n\|^2 = 0$ if and only if $z_{2n(M+1)\tau} = 1$, which holds if and only if $n(M+1)\tau \equiv 0 \pmod{\pi}$. \square

It can be checked that $nM\tau \equiv 0 \pmod{\pi}$ also yields $\langle \mathbf{u}_n, \mathbf{v}_n \rangle = 0$, but letting $n(M+1)\tau \equiv 0 \pmod{\pi}$ implies that $a_n \mathbf{u}_n + b_n \mathbf{v}_n$ is perpendicular to $b_n \mathbf{u}_n - a_n \mathbf{v}_n$ for all $a_n, b_n \in \mathbb{R}$. Now, to extend the perpendicularity results to components from different harmonics, we will use the following definition.

Definition 5.3 We say that a function f is L -periodic on $[0, 2\pi]$, $L \in \mathbb{N}$, if

$$f\left(t + \frac{2\pi}{L}\right) = f(t)$$

for all t .

Remark 5.4 If f is an L -periodic function, a_n and b_n are its n th real Fourier coefficients (see Eq. 2), and we let $a_n + ib_n = r_n e^{i\alpha_n}$, with $\alpha_n = 0$ whenever $r_n = 0$, then $r_n \neq 0$ implies $n \equiv 0 \pmod{L}$. Indeed, $g(t) = f(t/L)$ is a 1-periodic function and therefore has a Fourier series expansion

$$g(t) = \sum_{r=0}^{\infty} a'_r \cos(rt) + b'_r \sin(rt)$$

with equality almost everywhere. Thus,

$$f(t) = g(tL) = \sum_{r=0}^{\infty} a'_r \cos(rLt) + b'_r \sin(rLt) = \sum_{n=0}^{\infty} a_n \cos(nt) + b_n \sin(nt)$$

for almost every t , and the result follows from the uniqueness of the Fourier expansion in $L^2(\mathbb{T})$.

We are now ready to see that the potentially nonzero terms in the linear decomposition of $SW_{M,\tau} S_N f$ (Eq. 3) can be made mutually orthogonal by choosing the window size proportional to the underlying frequency, with proportionality constant $\frac{M}{M+1}$.

Proposition 5.5 *Let f be L -periodic, and let $\tau = \frac{2\pi}{L(M+1)}$. Then the vectors in*

$$\{\mathbf{u}_n, \mathbf{v}_n \mid 0 \leq n \leq N, n \equiv 0 \pmod{L}\}$$

are mutually orthogonal, and we have $\|\mathbf{u}_n\| = \|\mathbf{v}_n\| = \sqrt{\frac{M+1}{2}}$ for $n \equiv 0 \pmod{L}$.

Proof Let $k = pL$ and $n = qL$. If $k = n$, then it follows from Proposition 5.2 that $\langle \mathbf{u}_n, \mathbf{v}_n \rangle = 0$ and

$$\begin{aligned} \|\mathbf{u}_n\|^2 = \|\mathbf{v}_n\|^2 &= \frac{\|\mathbf{u}_n\|^2 + \|\mathbf{v}_n\|^2}{2} = \frac{1}{2} \sum_{m=0}^M \cos(nm\tau)^2 + \sin(nm\tau)^2 \\ &= \frac{M+1}{2}. \end{aligned}$$

Let us assume now that $p \neq q$. If we let $z_\theta = e^{i\theta}$, $\theta \in \mathbb{R}$, then

$$\begin{aligned} \langle \mathbf{u}_n, \mathbf{u}_k \rangle &= \sum_{m=0}^M \cos(nm\tau) \cos(km\tau) \\ &= \frac{1}{2} \sum_{m=0}^M \cos((n-k)m\tau) + \cos((n+k)m\tau) \\ &= \frac{1}{2} \operatorname{Re} \left(\frac{1 - z_{(n-k)(M+1)\tau}}{1 - z_{(n-k)\tau}} + \frac{1 - z_{(n+k)(M+1)\tau}}{1 - z_{(n+k)\tau}} \right) \\ &= \frac{1}{2} \operatorname{Re} \left(\frac{1 - z_{(q-p)2\pi}}{1 - z_{(n-k)\tau}} + \frac{1 - z_{(q+p)2\pi}}{1 - z_{(n+k)\tau}} \right) = 0. \end{aligned}$$

Notice that

$$0 < \min\{|n-k|, |n+k|\} \leq \max\{|n-k|, |n+k|\} \leq 2N \leq M < \frac{2\pi}{\tau}$$

implies that the denominators are never zero. Similarly,

$$\langle \mathbf{u}_n, \mathbf{v}_k \rangle = \sum_{m=1}^M \cos(nm\tau) \sin(km\tau)$$

$$\begin{aligned}
&= \frac{1}{2} \sum_{m=1}^M \sin((n+k)m\tau) - \sin((n-k)m\tau) \\
&= \frac{1}{2} \operatorname{Im} \left(\frac{1 - z_{(q+p)2\pi}}{1 - z_{(n+k)\tau}} - \frac{1 - z_{(q-p)2\pi}}{1 - z_{(n-k)\tau}} \right) = 0 \\
\langle \mathbf{v}_n, \mathbf{u}_k \rangle &= \frac{1}{2} \operatorname{Im} \left(\frac{1 - z_{(p+q)2\pi}}{1 - z_{(k+n)\tau}} - \frac{1 - z_{(p-q)2\pi}}{1 - z_{(k-n)\tau}} \right) = 0 \\
\langle \mathbf{v}_n, \mathbf{v}_k \rangle &= \frac{1}{2} \operatorname{Re} \left(\frac{1 - z_{(q-p)2\pi}}{1 - z_{(n-k)\tau}} - \frac{1 - z_{(q+p)2\pi}}{1 - z_{(n+k)\tau}} \right) = 0.
\end{aligned}$$

□

When computing persistent homology it is sometimes advantageous to pointwise center and normalize the set of interest. The next theorem describes the result of such operations on the sliding-window point cloud for $SW_{M,\tau} S_N f$ when f is L -periodic and $L(M+1)\tau = 2\pi$.

Theorem 5.6 (Structure) *Let $C : \mathbb{R}^{M+1} \rightarrow \mathbb{R}^{M+1}$ be the centering map*

$$C(\mathbf{x}) = \mathbf{x} - \frac{\langle \mathbf{x}, \mathbf{1} \rangle}{\|\mathbf{1}\|^2} \mathbf{1} \quad \text{where} \quad \mathbf{1} = \begin{bmatrix} 1 \\ \vdots \\ 1 \end{bmatrix} \in \mathbb{R}^{M+1}.$$

If f is L -periodic, $L(M+1)\tau = 2\pi$ and $\phi_\tau = SW_{M,\tau} S_N f$, then

(1)

$$\phi_\tau(t) = \widehat{f}(0) \cdot \mathbf{1} + C(\phi_\tau(t));$$

(2)

$$\|C(\phi_\tau(t))\| = \sqrt{M+1} \left(\|S_N f\|_2^2 - \widehat{f}(0)^2 \right)^{1/2};$$

(3) *There exists an orthonormal set*

$$\left\{ \tilde{\mathbf{x}}_n, \tilde{\mathbf{y}}_n \in \mathbb{R}^{M+1} \mid 1 \leq n \leq N, n \equiv 0 \pmod{L} \right\}$$

such that

$$\varphi_\tau(t) = \frac{C(\phi_\tau(t))}{\|C(\phi_\tau(t))\|} = \sum_{\substack{n=1 \\ n \equiv 0 \pmod{L}}}^N \tilde{r}_n (\cos(nt) \tilde{\mathbf{x}}_n + \sin(nt) \tilde{\mathbf{y}}_n), \quad (4)$$

where

$$\tilde{r}_n = \frac{2|\hat{f}(n)|}{\sqrt{\|S_N f\|_2^2 - \hat{f}(0)^2}}.$$

Proof If f is an L -periodic function on $[0, 2\pi]$ and $L(M+1)\tau = 2\pi$, then Remark 5.4 and Proposition 5.5 imply that for all $t \in \mathbb{R}$

$$\begin{aligned}\phi_\tau(t) &= \sum_{\substack{n=0 \\ n \equiv 0 \pmod{L}}}^N \cos(nt)(a_n \mathbf{u}_n + b_n \mathbf{v}_n) + \sin(nt)(b_n \mathbf{u}_n - a_n \mathbf{v}_n) \\ &= \sum_{\substack{n=0 \\ n \equiv 0 \pmod{L}}}^N r_n (\cos(nt) \mathbf{x}_n + \sin(nt) \mathbf{y}_n)\end{aligned}$$

is a linear combination of the mutually orthogonal vectors $\mathbf{x}_n = \cos(\alpha_n) \mathbf{u}_n + \sin(\alpha_n) \mathbf{v}_n$ and $\mathbf{y}_n = \sin(\alpha_n) \mathbf{u}_n - \cos(\alpha_n) \mathbf{v}_n$.

Moreover, from Proposition 5.5 we have that if $n \geq 1$ is such that $n \equiv 0 \pmod{L}$, then $\|\mathbf{x}_n\| = \|\mathbf{y}_n\| = \sqrt{\frac{M+1}{2}}$. It follows that if

$$\tilde{\mathbf{x}}_n = \frac{\mathbf{x}_n}{\|\mathbf{x}_n\|}, \quad \tilde{\mathbf{y}}_n = \frac{\mathbf{y}_n}{\|\mathbf{y}_n\|},$$

then

$$\phi_\tau(t) = (a_0 \sqrt{M+1}) \frac{\mathbf{1}}{\|\mathbf{1}\|} + \sum_{\substack{n=1 \\ n \equiv 0 \pmod{L}}}^N \sqrt{\frac{M+1}{2}} r_n (\cos(nt) \tilde{\mathbf{x}}_n + \sin(nt) \tilde{\mathbf{y}}_n)$$

is a linear decomposition of $\phi_\tau(t)$ in terms of the orthonormal set

$$\left\{ \frac{\mathbf{1}}{\|\mathbf{1}\|}, \tilde{\mathbf{x}}_n, \tilde{\mathbf{y}}_n \mid 1 \leq n \leq N, n \equiv 0 \pmod{L} \right\}.$$

Hence, $C(\phi_\tau(t)) = \sum_{\substack{n=1 \\ n \equiv 0 \pmod{L}}}^N \sqrt{\frac{M+1}{2}} r_n (\cos(nt) \tilde{\mathbf{x}}_n + \sin(nt) \tilde{\mathbf{y}}_n)$, and therefore

$$\begin{aligned}\varphi_\tau(t) &= \frac{C(\phi_\tau(t))}{\|C(\phi_\tau(t))\|} \\ &= \sum_{\substack{n=1 \\ n \equiv 0 \pmod{L}}}^N \frac{r_n}{\sqrt{r_1^2 + \cdots + r_N^2}} (\cos(nt) \tilde{\mathbf{x}}_n + \sin(nt) \tilde{\mathbf{y}}_n),\end{aligned}$$

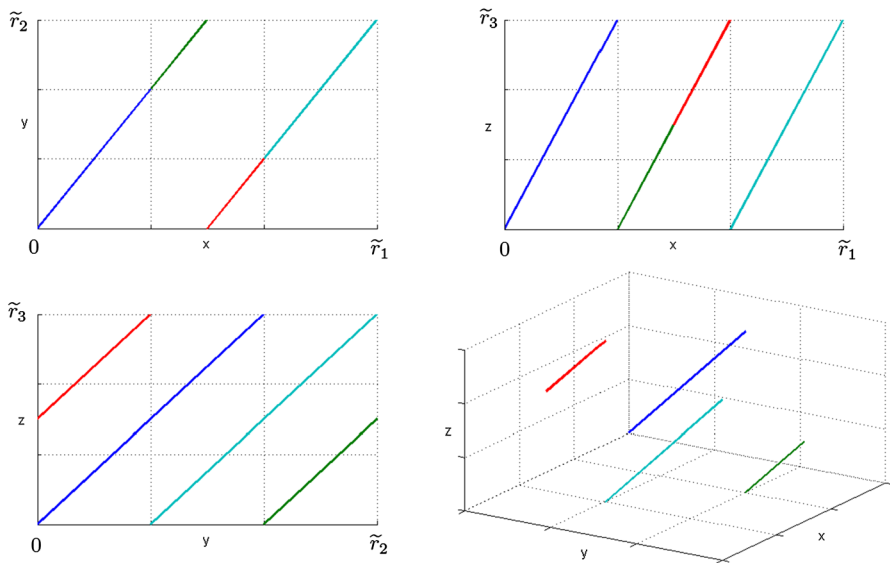


Fig. 2 The curve $\varphi_\tau(t)$, in colors, with respect to its flat coordinates $(t, 2t, 3t) \in (\mathbb{R}/\tilde{r}_1\mathbb{Z}) \times (\mathbb{R}/\tilde{r}_2\mathbb{Z}) \times (\mathbb{R}/\tilde{r}_3\mathbb{Z})$. Please refer to the electronic version for colors. *Bottom right* $\varphi_\tau(t)$ in fundamental domain $[0, \tilde{r}_1) \times [0, \tilde{r}_2) \times [0, \tilde{r}_3)$. *Top left* Projection onto xy -plane. *Top right* Projection onto xz -plane. *Bottom left* Projection onto yz -plane

which we write as

$$\varphi_\tau(t) = \sum_{\substack{n=1 \\ n \equiv 0 \pmod{L}}}^N \tilde{r}_n (\cos(nt) \tilde{\mathbf{x}}_n + \sin(nt) \tilde{\mathbf{y}}_n), \quad \sum_{n=1}^N \tilde{r}_n^2 = 1.$$

The result follows from the identities $r_n = 2 |\hat{f}(n)| = |\hat{f}(n)| + |\hat{f}(-n)|, n \geq 1$. \square

Theorem 5.6 allows us to paint a very clear geometric picture of the centered and normalized sliding-window point cloud for $S_N f$ (see Eq. 4). Indeed, if $S^1(r) \subset \mathbb{C}$ denotes the circle of radius r centered at zero, then $t \mapsto \varphi_\tau(t)$ can be regarded as the curve in the N -torus

$$\mathcal{T} = S^1(\tilde{r}_1) \times \cdots \times S^1(\tilde{r}_N),$$

which when projected onto $S^1(\tilde{r}_n)$, $\tilde{r}_n > 0$, goes around n times at a constant speed. Another interpretation, in terms of flat (polar) coordinates, is as the image through the quotient map

$$\mathbb{R}^N = \mathbb{R} \times \cdots \times \mathbb{R} \longrightarrow (\mathbb{R}/\tilde{r}_1\mathbb{Z}) \times \cdots \times (\mathbb{R}/\tilde{r}_N\mathbb{Z})$$

of the line segment in \mathbb{R}^N joining $(0, 0, \dots, 0)$ and $(\tilde{r}_1, 2\tilde{r}_2, \dots, N\tilde{r}_N)$. Figure 2 depicts $\varphi_\tau(t)$ inside \mathcal{T} for $N = 3$.

6 Persistent Homology of ϕ_τ and $SW_{M,\tau}f$

The structural observations from the previous section, as well as the approximation results from Sect. 4, set the stage for understanding the persistent homology of the image of ϕ_τ (or rather of φ_τ) and how it relates to that of $SW_{M,\tau}f$.

6.1 Some Convergence Results

Let $T \subset \mathbb{T}$, and let $SW_{M,\tau}f(T)$ and $\phi_\tau(T)$ be the images of T through $SW_{M,\tau}f$ and ϕ_τ , respectively. An immediate consequence of Proposition 4.2 is that as N (and thus $M = 2N$) gets larger, $\phi_\tau(T)$ gets closer to $SW_{M,\tau}f(T)$ with respect to the Hausdorff metric on subspaces of \mathbb{R}^∞ . Here \mathbb{R}^∞ denotes the set of sequences $x = (x_k)_{k \in \mathbb{N}}$, $x_k \in \mathbb{R}$, such that $x_n = 0$ for all $n \geq N_0$ and some $N_0 = N_0(x) \in \mathbb{N}$. We endow \mathbb{R}^∞ with the L^2 metric and regard $SW_{M,\tau}f(t)$, $t \in T$, as an element of \mathbb{R}^∞ by identifying it with

$$(f(t), f(t + \tau), \dots, f(t + M\tau), 0, 0, \dots) \in \mathbb{R}^\infty.$$

Notice, however, that while increasing the dimension $M + 1$ of the sliding-window embedding yields better approximations

$$SW_{M,\tau}S_Nf(T) \approx SW_{M,\tau}f(T),$$

the object being approximated, $SW_{M,\tau}f(T)$, is changing. Since $(\mathbb{R}^\infty, \|\cdot\|_2)$ is not complete, there is no reason to believe this process converges or stabilizes, even with a sensible way of comparing, say, $SW_{M,\tau}f(t)$ and $SW_{2M,\frac{\tau}{2}}f(t)$. This is the case since they are samplings at different rates from the same window. Perhaps considering the Gromov–Hausdorff distance instead of the Hausdorff distance would yield such a comparison, but at least at the moment we do not have a natural embedding to make this case. In addition, even when the metric completion $\overline{\mathbb{R}^\infty} = \ell^2(\mathbb{R})$, the space of square-summable sequences, is well understood, it is also large enough that tracking global geometric features requires some work. It is in situations like this that a succinct and informative summary, such as persistence diagrams, is critical.

It is known that the space of persistence diagrams is not complete with respect to the bottleneck distance but that it can be completed by allowing diagrams with countably many points with at most countable multiplicity, satisfying a natural finiteness condition. [See Theorem 3.4 in [2] and Theorem 6 in [19]]. Moreover, features such as maximum persistence can be easily tracked, and there is no ambiguity on how to compare the diagrams from, say, $SW_{M,\tau}f(T)$ and $SW_{2M,\frac{\tau}{2}}f(T)$.

Proposition 6.1 *Let f be L -periodic, $N < N'$, $M = 2N$, $M' = 2N'$, and*

$$\tau = \frac{2\pi}{L(M+1)}, \quad \tau' = \frac{2\pi}{L(M'+1)}.$$

If $T \subset \mathbb{T}$ is finite, $Y = SW_{M,\tau}S_Nf(T)$, and $Y' = SW_{M',\tau'}S_{N'}f(T)$, then

$$d_B \left(\frac{dgm(Y)}{\sqrt{M+1}}, \frac{dgm(Y')}{\sqrt{M'+1}} \right) \leq 2 \|S_N f - S_{N'} f\|_2,$$

where $\lambda \cdot dgm(Z)$ is defined as $\{(\lambda x, \lambda y) \mid (x, y) \in dgm(Z)\}$ for $\lambda \geq 0$.

Proof Let us fix the notation $\mathbf{u}_n = \mathbf{u}_n(M, \tau)$, $\mathbf{v}_n = \mathbf{v}_n(M, \tau)$, $\mathbf{u}'_n = \mathbf{u}_n(M', \tau')$, and $\mathbf{v}'_n = \mathbf{v}_n(M', \tau')$ in order to specify the dependencies of \mathbf{u}_n and \mathbf{v}_k on M and τ . Then we have the linear maps

$$P : \mathbb{R}^{M'+1} \longrightarrow \mathbb{R}^{M'+1} \\ \sum_{n=0}^{N'} x_n \mathbf{u}'_n + y_n \mathbf{v}'_n \mapsto \sum_{n=0}^N x_n \mathbf{u}'_n + y_n \mathbf{v}'_n,$$

$$Q : \text{Img}(P) \longrightarrow \mathbb{R}^{M+1} \\ \mathbf{u}'_n \mapsto \sqrt{\frac{M'+1}{M+1}} \mathbf{u}_n \\ \mathbf{v}'_n \mapsto \sqrt{\frac{M'+1}{M+1}} \mathbf{v}_n,$$

which are well defined by Proposition 5.1. Moreover, Proposition 5.5 implies that P can be interpreted as an orthogonal projection when restricted to Y' and that Q is an isometry on $P(Y')$. Notice that for every $y' \in Y'$

$$\|y' - P(y')\| = \sqrt{\frac{M'+1}{2} \sum_{n=N+1}^{N'} r_n^2},$$

where r_n is as defined in Remark 5.4, and therefore

$$d_H(Y', P(Y')) \leq \sqrt{\frac{M'+1}{2} \sum_{n=N+1}^{N'} r_n^2}.$$

Finally, since $Q \circ P(Y') = \sqrt{\frac{M'+1}{M+1}} Y$ and $dgm(\cdot)$ is invariant under isometries, then

$$\begin{aligned} \sqrt{M'+1} \cdot d_B \left(\frac{dgm(Y')}{\sqrt{M'+1}}, \frac{dgm(Y)}{\sqrt{M+1}} \right) &= d_B(dgm(Y'), dgm(Q \circ P(Y'))) \\ &= d_B(dgm(Y'), dgm(P(Y))) \\ &\leq 2d_H(Y', P(Y')) \\ &\leq \sqrt{2(M'+1) \sum_{n=N+1}^{N'} r_n^2}, \end{aligned}$$

and the result follows from the identity $r_n = 2|\widehat{f}(n)| = |\widehat{f}(n)| + |\widehat{f}(-n)|$, $n \geq 1$. \square

This result, paired with the fact that $\|f - S_N f\|_2 \rightarrow 0$ as $N \rightarrow \infty$ and the Structure Theorem 5.6(1), (2), implies the following corollary.

Corollary 6.2 *Let $f \in L^2(\mathbb{T})$ be L -periodic, $N \in \mathbb{N}$, $\tau_N = \frac{2\pi}{L(2N+1)}$, $T \subset \mathbb{T}$ finite, and let \tilde{Y}_N be the set resulting from pointwise centering and normalizing the point cloud*

$$SW_{2N, \tau_N} S_N f(T) \subset \mathbb{R}^{2N+1}.$$

Then for any field of coefficients, the sequence $\text{dgm}(\tilde{Y}_N)$ of persistence diagrams is Cauchy with respect to d_B .

Completeness of the set of (generalized) diagrams [2, Theorem 3.4], allows one to state the following definition.

Definition 6.3 Let $w = \frac{2\pi}{L}$, and denote by $\text{dgm}_\infty(f, T, w)$ the limit in the bottleneck distance of the sequence $\text{dgm}(\tilde{Y}_N)$.

We hope the notation $\text{dgm}_\infty(f, T, w)$ is suggestive enough to evoke the idea that there exists a limiting diagram from the sequence of pointwise-centered and normalized versions of $SW_{M, \tau} f(T)$, as $M \rightarrow \infty$, and while keeping the window size $M\tau = \frac{M}{M+1}w \approx w$. The first convergence theorem (Theorem 6.6) below asserts the validity of this notation. Before presenting the proof, we start with a technical result.

Proposition 6.4 *Let $f \in C(\mathbb{T})$ be L -periodic, $N \in \mathbb{N}$, and $\tau_N = \frac{2\pi}{L(2N+1)}$. Then*

$$\lim_{N \rightarrow \infty} \frac{\|C(SW_{2N, \tau_N} f(t))\|}{\sqrt{2N+1}} = \|f - \hat{f}(0)\|_2 \quad (5)$$

uniformly in $t \in \mathbb{T}$.

Proof Since the result is trivially true if f is constant, let us assume $f \neq \hat{f}(0)$, and let

$$g(t) = \frac{f(t) - \hat{f}(0)}{\|f - \hat{f}(0)\|_2}.$$

It follows that $g \in C(\mathbb{T})$ is L -periodic,

$$\hat{g}(0) = \frac{1}{2\pi} \int_0^{2\pi} g(t) dt = 0 \quad \text{and} \quad \|g\|_2 = \frac{1}{\sqrt{2\pi}} \left(\int_0^{2\pi} |g(t)|^2 dt \right)^{1/2} = 1.$$

Using the identity $L(2N+1)\tau_N = 2\pi$, a Riemann sums argument, and the fact that g is L -periodic, it follows that if

$$c_N(t) = \frac{g(t) + g(t + \tau_N) + \cdots + g(t + 2N\tau_N)}{2N+1},$$

then for all $t \in \mathbb{T}$

$$\begin{aligned} \lim_{N \rightarrow \infty} c_N(t) &= \lim_{\tau_N \rightarrow 0} \frac{L}{2\pi} \left(\tau_N g(t) + \tau_N g(t + \tau_N) + \cdots + \tau_N g(t + 2N\tau_N) \right) \\ &= \frac{L}{2\pi} \int_t^{t + \frac{2\pi}{L}} g(r) dr \\ &= \frac{1}{2\pi} \int_0^{2\pi} g(r) dr \\ &= 0. \end{aligned}$$

We contend that the convergence $c_N(t) \rightarrow 0$ is uniform in $t \in \mathbb{T}$. Indeed, the fact that g is uniformly continuous implies that the sequence $c_N(t)$ is uniformly equicontinuous. This means that for every $\epsilon > 0$ there exists $\delta > 0$ independent of N such that for every $t, t' \in \mathbb{T}$ and all $N \in \mathbb{N}$

$$|t - t'| < \delta \text{ implies } |c_N(t) - c_N(t')| < \frac{\epsilon}{2}.$$

Let $N_t \in \mathbb{N}$, for $t \in \mathbb{T}$, be such that $N \geq N_t$ implies $|c_N(t)| < \frac{\epsilon}{2}$. These two inequalities together imply that if $N \geq N_t$ and $|t - t'| < \delta$, then $|c_N(t')| < \epsilon$.

By choosing a finite open cover of $[0, 2\pi]$ with intervals of length δ and letting N_0 be the maximum of the N_t corresponding to their centers, we get that $N \geq N_0$ implies $|c_N(t)| < \epsilon$ for all $t \in \mathbb{T}$. Thus, the convergence $c_N(t) \rightarrow 0$ is uniform. A similar argument shows that

$$\begin{aligned} \lim_{N \rightarrow \infty} \frac{\|C(SW_{2N, \tau_N} g(t))\|^2}{2N + 1} &= \lim_{\tau_N \rightarrow 0} \frac{L}{2\pi} \sum_{n=0}^{2N} \tau_N (g(t + n\tau_N) - c_N(t))^2 \\ &= \frac{1}{2\pi} \int_0^{2\pi} g(r)^2 dr = 1 \end{aligned}$$

uniformly in $t \in \mathbb{T}$, and replacing g by $\frac{f - \hat{f}(0)}{\|f - \hat{f}(0)\|_2}$ yields the result. \square

Remark 6.5 Notice that an alternative proof of Proposition 6.4 follows from combining the Structure Theorem 5.6(2), Parseval's Theorem, and the fact that

$$\|S_N f\|_2^2 - \hat{f}(0)^2 = \|S_N (f - \hat{f}(0))\|_2^2.$$

Theorem 6.6 (Convergence I) *Let $f \in C^1(\mathbb{T})$ be an L -periodic function, $N \in \mathbb{N}$, $\tau_N = \frac{2\pi}{L(2N+1)}$, $T \subset \mathbb{T}$ finite, and let \tilde{Y}_N be as in Corollary 6.2. Let \tilde{X}_N be the set resulting from pointwise centering and normalizing the point cloud*

$$SW_{2N, \tau_N} f(T) \subset \mathbb{R}^{2N+1}.$$

Then for any field of coefficients, the sequence $\text{dgm}(\bar{X}_N)$ of persistence diagrams is Cauchy with respect to d_B , and

$$\lim_{N \rightarrow \infty} \text{dgm}(\bar{X}_N) = \lim_{N \rightarrow \infty} \text{dgm}(\bar{Y}_N) = \text{dgm}_\infty(f, T, w).$$

Proof To prove Theorem 6.6, we will use the Approximation Theorem 4.5 to show that

$$\lim_{N \rightarrow \infty} d_B(\text{dgm}(\bar{X}_N), \text{dgm}(\bar{Y}_N)) = 0$$

and combine this with Corollary 6.2 to obtain the result.

Assume without loss of generality that f satisfies $\hat{f}(0) = 0$ and $\|f\|_2 = 1$. Let X_N and Y_N be the resulting sets from pointwise centering the point clouds $SW_{2N, \tau_N} f(T)$ and $SW_{2N, \tau_N} S_N f(T)$, respectively. Using the uniform convergence in Eq. 5 we get that

$$\lim_{N \rightarrow \infty} d_H\left(\bar{X}_N, \frac{X_N}{\sqrt{2N+1}}\right) = 0,$$

and moreover, since $\lim_{N \rightarrow \infty} \|S_N f\|_2 = \|f\|_2 = 1$, then

$$\lim_{N \rightarrow \infty} d_H\left(\frac{X_N}{\sqrt{2N+1}}, \frac{X_N}{\sqrt{2N+1}\|S_N f\|_2}\right) = 0.$$

Now, from the Structure Theorem 5.6(2) we have the identity

$$\bar{Y}_N = \frac{Y_N}{\sqrt{2N+1}\|S_N f\|_2},$$

and using the Approximation Theorem 4.5(1), along with the fact that C is distance nonincreasing, we conclude that

$$\lim_{N \rightarrow \infty} d_H\left(\frac{X_N}{\sqrt{2N+1}\|S_N f\|_2}, \bar{Y}_N\right) \leq \lim_{N \rightarrow \infty} \frac{\sqrt{2} \cdot \|R_N f'\|_2}{\|S_N f\|_2 \cdot \sqrt{N+1}} = 0.$$

The triangular inequality then implies that $\lim_{N \rightarrow \infty} d_H(\bar{X}_N, \bar{Y}_N) = 0$, and the result follows from combining the stability of d_B with respect to d_H and Corollary 6.2. \square

The first convergence theorem asserts that for each choice of discretization $T \subset \mathbb{T}$ one obtains a limiting diagram $\text{dgm}_\infty(f, T, w)$ by letting $N \rightarrow \infty$ in the pointwise centered and normalized versions of either $SW_{2N, \tau_N} S_N f(T)$ or $SW_{2N, \tau_N} f(T)$. Next we will show that there is also convergence when T tends to \mathbb{T} with respect to the Hausdorff distance on subspaces of \mathbb{T} .

Theorem 6.7 (Convergence II) *Let $T, T' \subset \mathbb{T}$ be finite, and let $f \in C^1(\mathbb{T})$ be L -periodic with modulus of continuity $\omega : [0, \infty] \rightarrow [0, \infty]$. If $w = \frac{2\pi}{L}$, then*

$$d_B(dgm_\infty(f, T, w), dgm_\infty(f, T', w)) \leq 2 \|f - \widehat{f}(0)\|_2 \omega(d_H(T, T')),$$

and thus there exists a persistence diagram $dgm_\infty(f, w)$ so that

$$\lim_{T \rightarrow \mathbb{T}} dgm_\infty(f, T, w) = dgm_\infty(f, w).$$

Proof Fix $t \in T$ and $t' \in T'$. If we let $\mathbf{x}_N = SW_{2N, \tau_N} f(t)$, $\mathbf{x}'_N = SW_{2N, \tau_N} f(t')$, $\tau_N = \frac{2\pi}{L(2N+1)}$, and $\lambda = \|f - \widehat{f}(0)\|_2$, then

$$\begin{aligned} \left\| \frac{C(\mathbf{x}_N)}{\|C(\mathbf{x}_N)\|} - \frac{C(\mathbf{x}'_N)}{\|C(\mathbf{x}'_N)\|} \right\| &\leq \left\| \frac{C(\mathbf{x}_N)}{\|C(\mathbf{x}_N)\|} - \frac{\lambda C(\mathbf{x}_N)}{\sqrt{2N+1}} \right\| + \frac{\lambda \|C(\mathbf{x}_N) - C(\mathbf{x}'_N)\|}{\sqrt{2N+1}} \\ &\quad + \left\| \frac{C(\mathbf{x}'_N)}{\|C(\mathbf{x}'_N)\|} - \frac{\lambda C(\mathbf{x}'_N)}{\sqrt{2N+1}} \right\|. \end{aligned}$$

It follows from Proposition 6.4 that both the summand

$$\left\| \frac{C(\mathbf{x}_N)}{\|C(\mathbf{x}_N)\|} - \frac{\lambda C(\mathbf{x}_N)}{\sqrt{2N+1}} \right\| = \frac{\|C(\mathbf{x}_N)\|}{\sqrt{2N+1}} \cdot \left| \frac{\sqrt{2N+1}}{\|C(\mathbf{x}_N)\|} - \lambda \right|$$

and its version with \mathbf{x}'_N go to zero as $N \rightarrow \infty$. Thus, given $\epsilon > 0$, there exists $N_0 \in \mathbb{N}$ such that $N \geq N_0$ implies

$$\begin{aligned} \left\| \frac{C(\mathbf{x}_N)}{\|C(\mathbf{x}_N)\|} - \frac{C(\mathbf{x}'_N)}{\|C(\mathbf{x}'_N)\|} \right\| &\leq \frac{\epsilon}{2} + \frac{\lambda \|C(\mathbf{x}_N) - C(\mathbf{x}'_N)\|}{\sqrt{2N+1}} \\ &\leq \frac{\epsilon}{2} + \frac{\lambda \|\mathbf{x}_N - \mathbf{x}'_N\|}{\sqrt{2N+1}} \\ &= \frac{\epsilon}{2} + \lambda \left(\sum_{n=0}^{2N} \frac{|f(t + n\tau_N) - f(t' + n\tau_N)|^2}{2N+1} \right)^{1/2} \\ &\leq \frac{\epsilon}{2} + \lambda \omega(|t - t'|). \end{aligned}$$

Let \bar{X}_N and \bar{X}'_N be the sets resulting from pointwise centering and normalizing $SW_{2N, \tau_N} f(T)$ and $SW_{2N, \tau_N} f(T')$, respectively. Since the preceding estimates are uniform in t and t' (by Proposition 6.4), it follows that whenever $N \geq N_0$,

$$d_H(\bar{X}_N, \bar{X}'_N) \leq \frac{\epsilon}{2} + \lambda \omega(d_H(T, T')).$$

Notice that the Hausdorff distance on the left-hand side is for subspaces of \mathbb{R}^{2N+1} , while that on the right-hand side is between subspaces of \mathbb{T} .

Applying the stability theorem for persistence diagrams yields

$$d_B(\text{dgm}(\bar{X}_N), \text{dgm}(\bar{X}'_N)) \leq \epsilon + 2\lambda\omega(d_H(T, T')),$$

which, by letting $N \rightarrow \infty$ and applying the first convergence theorem (Theorem 6.6), implies

$$d_B(\text{dgm}_\infty(f, T, w), \text{dgm}_\infty(f, T', w)) \leq \epsilon + 2\lambda\omega(d_H(T, T')).$$

Since this is true for any $\epsilon > 0$, letting $\epsilon \downarrow 0$ yields the first part of the theorem. The existence of $\text{dgm}_\infty(f, w)$ follows from the fact that the set of generalized persistence diagrams is complete with respect to d_B . \square

6.2 A Lower Bound for Maximum Persistence

The structure theorem, Theorem 5.6(3), and the fact that orthogonal projections are distance nonincreasing allow us to now prove the following theorem.

Theorem 6.8 *Let $f \in C^1(\mathbb{T})$ be an L -periodic function, $N \in \mathbb{N}$, $M \geq 2N$, $L(M+1)\tau = 2\pi$, and let $T \subset \mathbb{T}$ be finite. Furthermore, assume that $d_H(T, \mathbb{T}) < \delta$ for some [see Theorem 5.6(3)]*

$$0 < \delta < \max_{1 \leq n \leq N} \frac{\sqrt{3}\tilde{r}_n}{\kappa_N}, \text{ where } \kappa_N = \frac{2\sqrt{2} \|S_N f'\|_2}{\|S_N(f - \widehat{f}(0))\|_2}.$$

Let $\bar{Y} = \bar{Y}_N$ be the set resulting from pointwise centering and normalizing the point cloud

$$SW_{M,\tau} S_N f(T) \subset \mathbb{R}^{M+1},$$

and let $p > N$ be a prime. If $\text{dgm}(\bar{Y})$ denotes the 1D \mathbb{F}_p -persistence diagram for the Rips filtration on \bar{Y} , then φ_τ yields an element $\mathbf{x}_\varphi \in \text{dgm}(\bar{Y})$, with

- (1) $\text{birth}(\mathbf{x}_\varphi) \leq \delta\kappa_N$,
- (2) $\text{death}(\mathbf{x}_\varphi) \geq \sqrt{3} \max_{1 \leq n \leq N} \tilde{r}_n$,

and therefore

$$mp(\text{dgm}(\bar{Y})) \geq \left(\sqrt{3} \max_{1 \leq n \leq N} \tilde{r}_n \right) - \delta\kappa_N. \quad (6)$$

Proof Given the linear decomposition

$$\varphi_\tau(t) = \sum_{\substack{n=1 \\ n \equiv 0 \pmod{L}}}^N \tilde{r}_n (\cos(nt)\tilde{\mathbf{x}}_n + \sin(nt)\tilde{\mathbf{y}}_n)$$

of $\varphi_\tau(t)$ with respect to the orthonormal set $\{\tilde{\mathbf{x}}_n, \tilde{\mathbf{y}}_n \mid 1 \leq n \leq N, n \equiv 0 \pmod{L}\}$ described in the proof of Theorem 5.6(3), it follows that

$$\begin{aligned} P_n : \bar{Y} &\longrightarrow \mathbb{C} \\ \varphi_\tau(t) &\mapsto \tilde{r}_n e^{int} \end{aligned}$$

can be regarded as the restriction to \bar{Y} of the orthogonal projection from \mathbb{R}^{M+1} onto $\text{Span}\{\tilde{\mathbf{x}}_n, \tilde{\mathbf{y}}_n\}$. Since orthogonal projections are linear and norm-non-increasing, then $\|P_n(\mathbf{x}) - P_n(\mathbf{y})\| \leq \|\mathbf{x} - \mathbf{y}\|$ for every $\mathbf{x}, \mathbf{y} \in \bar{Y}$. Thus, if

$$S^1(\tilde{r}_n) = \{\tilde{r}_n e^{int} \mid t \in T\},$$

then it follows that P_n induces simplicial maps

$$\begin{aligned} P_{n\sharp} : R_\epsilon(\bar{Y}) &\longrightarrow R_\epsilon(S^1(\tilde{r}_n)) \\ [\mathbf{x}_0, \dots, \mathbf{x}_k] &\mapsto [P_n(\mathbf{x}_0), \dots, P_n(\mathbf{x}_k)] \end{aligned}$$

for every $\epsilon > 0$, which in turn yield homomorphisms

$$P_{n*} : H_k(R_\epsilon(\bar{Y}); \mathbb{F}_p) \longrightarrow H_k(R_\epsilon(S^1(\tilde{r}_n)); \mathbb{F}_p)$$

of \mathbb{F}_p -vector spaces at the homology level. What we contend is that, via the homomorphisms P_{n*} , the maximum 1D persistence of \bar{Y} can be bounded below by that of $S^1(\tilde{r}_n)$. Indeed, let $\epsilon_1, \epsilon_2 > 0$ be such that

$$\delta\kappa_N < \epsilon_1 < \epsilon_2 < \sqrt{3}\tilde{r}_m,$$

where $m = \arg \max \{\tilde{r}_n \mid 1 \leq n \leq N\}$. If we write

$$T = \{t_0 < t_2 < \dots < t_J\},$$

then it follows from $d_H(T, \mathbb{T}) < \delta$ that $|t_j - t_{j-1}| < 2\delta$ for all $j = 1, \dots, J$, and therefore

$$\begin{aligned} \|\varphi_\tau(t_j) - \varphi_\tau(t_{j-1})\|^2 &= \sum_{\substack{n=1 \\ n \equiv 0 \pmod{L}}}^N 2\tilde{r}_n^2 \left(1 - \cos(n(t_j - t_{j-1}))\right) \\ &\leq \sum_{\substack{n=1 \\ n \equiv 0 \pmod{L}}}^N \tilde{r}_n^2 (n(t_j - t_{j-1}))^2 \\ &= (t_j - t_{j-1})^2 \sum_{n=1}^N \frac{4n^2 |\widehat{f}(n)|^2}{\|S_N f\|_2^2 - \widehat{f}(0)^2} \end{aligned}$$

$$\begin{aligned}
 &= \frac{(t_j - t_{j-1})^2}{\|S_N(f - \widehat{f}(0))\|_2^2} \sum_{1 \leq |n| \leq N} 2 |\widehat{f}'(n)|^2 \\
 &\leq 8\delta^2 \frac{\|S_N f'\|_2^2}{\|S_N(f - \widehat{f}(0))\|_2^2} \\
 &= (\delta\kappa_N)^2.
 \end{aligned}$$

The first inequality is a consequence of the Taylor expansion for $\cos(x)$ around zero, and f' denotes the first derivative of f .

Therefore,

$$v = [\varphi_\tau(t_0), \varphi_\tau(t_1)] + \cdots + [\varphi_\tau(t_{J-1}), \varphi_\tau(t_J)] + [\varphi_\tau(t_J), \varphi_\tau(t_0)]$$

is a 1D cycle on $R_{\epsilon_1}(\bar{Y})$, and we obtain the homology class

$$P_{m*}([v]) \in H_1\left(R_{\epsilon_1}\left(S^1(\tilde{r}_m)\right); \mathbb{F}_p\right).$$

Let $\{\theta_0 < \theta_1 < \cdots < \theta_{J_m}\} = \{t \bmod \frac{2\pi}{m} \mid t \in T\}$ and let $c_j = \tilde{r}_m e^{im\theta_j}$. It follows from a similar calculation that

$$\|c_j - c_{j-1}\|^2 \leq (\theta_j - \theta_{j-1})^2 \frac{4 |\widehat{f}'(m)|^2}{\|S_N(f - \widehat{f}(0))\|_2^2} \leq (\delta\kappa_N)^2,$$

and therefore the 1-cycle

$$\mu = [c_0, c_1] + \cdots + [c_{J_m-1}, c_{J_m}] + [c_{J_m}, c_0]$$

is such that its homology class $[\mu] \in H_1(R_{\epsilon_1}(S^1(\tilde{r}_m)); \mathbb{F}_p)$ satisfies $i_*([\mu]) \neq 0$, where i_* is the homomorphism induced by the inclusion

$$i : R_{\epsilon_1}(S^1(\tilde{r}_m)) \hookrightarrow R_{\epsilon_2}(S^1(\tilde{r}_m)).$$

Since $P_{m*}([v]) = m[\mu]$, and given that $1 \leq m \leq N < p$ implies that m is invertible in \mathbb{F}_p , $i_* \circ P_{m*}([v]) \neq 0$. From the commutativity of the diagram

$$\begin{array}{ccc}
 H_1(R_{\epsilon_1}(\bar{Y}); \mathbb{F}_p) & \xrightarrow{i_*} & H_1(R_{\epsilon_2}(\bar{Y}); \mathbb{F}_p) \\
 P_{m*} \downarrow & & \downarrow P_{m*} \\
 H_1(R_{\epsilon_1}(S^1(\tilde{r}_m)); \mathbb{F}_p) & \xrightarrow{i_*} & H_1(R_{\epsilon_2}(S^1(\tilde{r}_m)); \mathbb{F}_p)
 \end{array}$$

we conclude that $i_*([v]) \neq 0$, and thus $[v]$ yields an element $\mathbf{x}_\varphi \in \mathbf{dgm}(\bar{Y})$ such that

$$\text{birth}(\mathbf{x}_\varphi) \leq \epsilon_1 \quad \text{and} \quad \text{death}(\mathbf{x}_\varphi) \geq \epsilon_2.$$

Given that this is true for every $\epsilon_1 > \delta\kappa_N$ and every $\epsilon_2 < \sqrt{3}\tilde{r}_m$, letting $\epsilon_1 \downarrow \delta\kappa_N$ and $\epsilon_2 \uparrow \sqrt{3}\tilde{r}_m$ concludes the proof. \square

Remark 6.9 It is worth noting that in the proof of Theorem 6.8 one can replace \mathbb{F}_p , $p > N$, by the field of rational numbers \mathbb{Q} . That is, the estimated bound for maximum persistence is valid for all $N \in \mathbb{N}$ and homology with \mathbb{Q} coefficients.

Equation 6, together with the Convergence Theorems I (Theorem 6.6) and II (Theorem 6.7), implies the following corollary.

Corollary 6.10 *Let $f \in C^1(\mathbb{T})$ be an L -periodic function such that $\widehat{f}(0) = 0$ and $\|f\|_2 = 1$. Let $T \subset \mathbb{T}$ be finite and such that $d_H(T, \mathbb{T}) < \delta$ for some*

$$0 < \delta < \frac{\sqrt{3}}{\sqrt{2}\|f'\|_2} \max_{n \in \mathbb{N}} |\widehat{f}(n)|.$$

Then with \mathbb{Q} coefficients, the 1D persistence diagram $dgm_\infty(f, T, w)$ satisfies

$$\frac{1}{2}mp(dgm_\infty(f, T, w)) \geq \sqrt{3} \max_{n \in \mathbb{N}} |\widehat{f}(n)| - \sqrt{2}\delta\|f'\|_2,$$

and therefore

$$mp(dgm_\infty(f, w)) \geq 2\sqrt{3} \max_{n \in \mathbb{N}} |\widehat{f}(n)|.$$

6.3 Field of Coefficients

One question worth asking is whether the lower bound for maximum persistence presented in Theorem 6.8 is in fact dependent on the field of coefficients. More generally, one would like to determine whether the full persistence diagram has such a dependency. To this end, let us consider the functions

$$\begin{aligned} g_1(t) &= 0.6 \cos(t) + 0.8 \cos(2t), \\ g_2(t) &= 0.8 \cos(t) + 0.6 \cos(2t). \end{aligned}$$

We construct their associated sliding-window point clouds, $SW_{M,\tau}g_1(T)$ and $SW_{M,\tau}g_2(T)$, using $M = 4$, $\tau = 2\pi/5$, and $T = \{\frac{2\pi k}{150} \mid k = 0, 1, \dots, 150\}$. After pointwise centering and normalizing, we compute their 1D persistent homology with coefficients in \mathbb{F}_2 and \mathbb{F}_3 . For this we use a fast implementation of the 1D persistent homology, based on the Union–Find algorithm and the work of Mischaikow and Nanda [20]. Details of this implementation will appear in [23].

We summarize the results in Fig. 3.

This example shows that, at least in low dimensions, the persistent homology of sliding-window point clouds is coefficient-dependent. Let us see why this is so. If

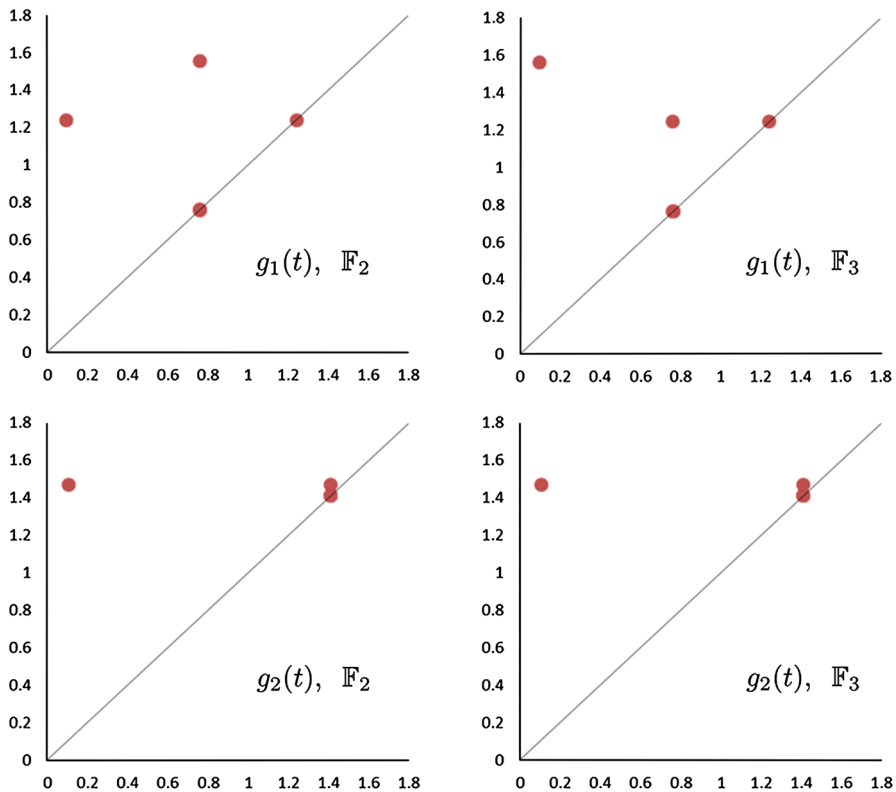


Fig. 3 One-dimensional \mathbb{F}_p -persistence diagrams for centered and normalized sliding-window point clouds on g_i . Here the columns correspond to $p = 2, 3$ and the rows to $i = 1, 2$

$(r_1, r_2) \in \mathbb{R}^2$ is such that $r_1^2 + r_2^2 = 1$ and $r_1 r_2 \neq 0$, it follows from the Structure Theorem 5.6(3) that if $\alpha_1, \alpha_2 \in [0, 2\pi]$ and

$$g(t) = r_1 \cos(t - \alpha_1) + r_2 \cos(2t - \alpha_2),$$

then for every $t \in [0, 2\pi]$ and $M \geq 4$, $\tau = \frac{2\pi}{M+1}$, one has that

$$\varphi_\tau(t) = \frac{C(SW_{M,\tau}g(t))}{\|C(SW_{M,\tau}g(t))\|}$$

can be isometrically identified with

$$\tilde{\varphi}(t) = (r_1 e^{it}, r_2 e^{2it}) \in \mathbb{C}^2.$$

Let us use $\tilde{\varphi}$ instead of φ_τ for the persistent homology computation. The first thing to notice is that the image of $\tilde{\varphi}$ can be realized as the boundary of a Möbius strip. Indeed, consider the map

$$\begin{aligned}\mathcal{M}: [0, \pi] \times [-1, 1] &\longrightarrow \mathbb{C}^2 \\ (t, s) &\longmapsto (-sr_1 e^{it}, r_2 e^{2it}).\end{aligned}$$

It follows that \mathcal{M} is a continuous injection on $[0, \pi] \times [-1, 1]$, since $r_1 r_2 \neq 0$, and that it descends to an embedding of the quotient space

$$\widetilde{\mathcal{M}}: ([0, \pi] \times [-1, 1] / \sim) \longrightarrow \mathbb{C}^2,$$

where $(0, s) \sim (\pi, -s)$ for every $s \in [-1, 1]$. Notice that $[0, \pi] \times [-1, 1] / \sim$ serves as the usual model for the Möbius strip and that $\partial(\text{Img}(\widetilde{\mathcal{M}})) = \text{Img}(\widetilde{\varphi})$.

Let $T = \{t_0 < t_2 < \cdots < t_J\}$ be a δ -dense subset of $[0, 2\pi]$, $X = \widetilde{\varphi}(T)$, and let

$$[v] \in H_1(R_r(X); \mathbb{F}_2),$$

for $r > 4\delta$, be the homology class of the 1-cycle

$$v = [\widetilde{\varphi}(t_0), \widetilde{\varphi}(t_1)] + \cdots + [\widetilde{\varphi}(t_{J-1}), \widetilde{\varphi}(t_J)] + [\widetilde{\varphi}(t_J), \widetilde{\varphi}(t_0)].$$

It can be readily verified that if we let

$$V = \left\{ (t, s) \mid (t, s) \in (T \cap [0, \pi)) \times \{-1\} \text{ or } (t + \pi, s) \in (T \cap (\pi, 2\pi]) \times \{1\} \right\},$$

then there exists a triangulation of $\text{Img}(\widetilde{\mathcal{M}})$ having $\widetilde{\mathcal{M}}(V)$ as vertex set, and so if we take coefficients in \mathbb{F}_2 , then the formal sum of its triangles yields a 2-chain Σ with $\partial_2(\Sigma) = v$. Moreover, since T is δ -dense in $[0, 2\pi]$ and for all $t \in [0, \pi]$

$$\begin{aligned}\|\widetilde{\mathcal{M}}(t, -1) - \widetilde{\mathcal{M}}(t \pm \delta, 1)\|^2 &= 2[r_1^2(1 + \cos(\delta)) + r_2^2(1 - \cos(2\delta))] \\ &\leq 2\left[r_1^2\left(2 - \frac{\delta^2}{2}\right) + 2r_2^2\delta^2\right] \\ &= r_1^2(4 - 5\delta^2) + 4\delta^2,\end{aligned}$$

if $\delta > 0$ is small, then we can choose Σ such that

$$\Sigma \in C_2(R_{r'}(X); \mathbb{F}_2), \quad r' = r_1\sqrt{4 - 5\delta^2} + 2\delta.$$

In summary, if

$$r_1\sqrt{4 - 5\delta^2} + 2\delta < \sqrt{3}r_2, \quad (7)$$

then the death time of the class $[v]$ is less than or equal to $r_1\sqrt{4 - 5\delta^2} + 2\delta$, with coefficients in \mathbb{F}_2 , but larger than $\sqrt{3}r_2$ (by Theorem 6.8), with coefficients in \mathbb{F}_p for any prime $p \geq 3$. Moreover, with coefficients in \mathbb{F}_2 and provided Eq. 7 holds (e.g., for g_1), the first edge across the Möbius band prompts the birth of a new class corresponding to the equator

$$t \mapsto \widetilde{\mathcal{M}}(t, 0) = (0, r_2 e^{2it})$$

of the embedded Möbius strip. This class in turn survives up to $\sqrt{3}r_2$. With coefficients in \mathbb{F}_3 , on the other hand, the equatorial and boundary classes will be in the same persistence class once all the 2-simplices in the Möbius band have been added. This results in the death of the class that was born later, i.e., the one represented by the equator.

7 Examples: Quantifying Periodicity of Sampled Signals

We present in this section two experiments to test our ideas: first, the ranking of signals by periodicity alone, in a way that is invariant to the shape of the periodic pattern, and second, the accurate classification of a signal as periodic or nonperiodic at different noise levels. A detailed description of our methods is provided below, but roughly speaking, we associate to each sampled signal $S = [s_1, \dots, s_J]$ a real-valued function f_S by cubic spline interpolation, construct its centered and normalized sliding-window point cloud X_S , and let

$$\frac{mp(\text{dgm}(X_S))}{\sqrt{3}} = \text{Score}(S)$$

be its periodicity score. We then compare it to those obtained with the JTK_CYCLE [15], Lomb–Scargle [13, 18, 24], and total persistent homology [7] algorithms.

7.1 Shape Independence

For this experiment we construct ten different shapes: a 2-periodic pure cosinelike curve, a 2-periodic cosinelike function plus three levels of gaussian noise (variances at 25, 50, and 75 % of signal amplitude), a noisy sawtooth (noise level at 25 % of signal amplitude), a function of the form $\cos(\phi(t))$ for $\phi(t) = e^{at+b}$, a noisy and damped cosinelike curve with three periods, a spiky signal with three periods, a noisy square wave with two periods, and a 1-periodic function of the form $\text{Re} \left(\sum_{n=1}^5 \hat{f}(n) e^{2\pi i n t} \right)$ for $\hat{f}(n)$ drawn randomly and uniformly from the unit disk in \mathbb{C} . Each function is then evaluated at 50 evenly spaced time points, yielding the sampled signals $[s_1, \dots, s_{50}]$ that we input into the algorithms. For the construction of the sliding-window point clouds we use $N = 10$, coefficients in \mathbb{F}_{11} , $L = 2, 3, 4$, and report the best score. In all the other algorithms we set the parameters to their suggested or default values. The results are summarized in Fig. 4.

Two things are worth noting. First, except for the sliding-window method (SWIPerS), all other algorithms have clear preferences for the type of shape they consider to be most periodic. These biases are of course part of the wiring of the algorithms and were to be expected. The second thing to notice has to do with the distribution of scores and their relative differences. Methods such as JTK or Lomb–Scargle define their periodicity score in terms of p -values, which are extremely difficult to interpret.

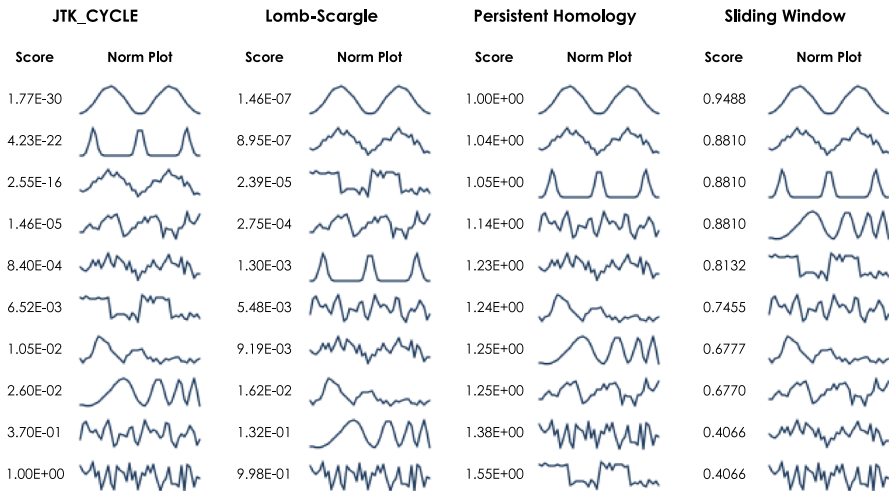


Fig. 4 Ranking of signals by periodicity. For each algorithm we provide the score and a normalized plot of the signal. The ranking goes from *top* (highest score) to *bottom* (lowest score)

Our scoring method, by way of contrast, has a clear geometric interpretation and a reasonable distribution.

7.2 Classification Rates

We compare the different algorithms by their ability to separate periodic from nonperiodic signals. The performance of this type of binary classification can be visualized using a receiver operating characteristic (ROC) plot, which compares the true positive rate (TPR) to the false positive rate (FPR) as a cutoff on the scores is varied. Here the TPR is the proportion of correctly identified positive cases out of all positives, and FPR is the proportion of negative cases incorrectly identified as positives out of all the negatives. The line $TPR = FPR$ is the performance of random guessing; the higher the ROC curve is above this line, the better its classification performance. An algorithm that is able to perfectly separate all positive from negative test cases would have a ROC curve that passes through the point $TPR = 1$ and $FPR = 0$. It follows that a reasonable measure of classification success for a particular method is the area under its ROC curves.

The synthetic data are generated as follows: the periodic signals (positive cases) span two periods and include a cosine, cosine with trending, cosine with damping, and cosine with increased peak steepness. The nonperiodic signals (negative cases) include a constant and a linear function. We generate 100 profiles from each shape by adjusting its phase. For instance, in the case of the cosine shape we let

$$f_j(t) = \cos\left(2t - \frac{j\pi}{50}\right), \quad j = 0, \dots, 99$$

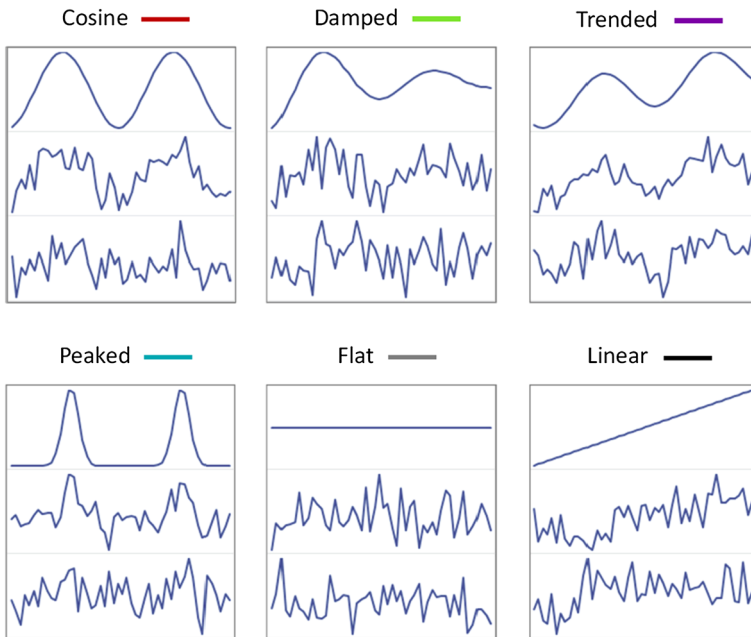


Fig. 5 Examples of signals in synthetic data. We show one signal from each profile type at noise levels 0, 25, and 50 %

be the profiles. We sample each of the 600 profiles at 50 evenly spaced time points $t \in [0, 2\pi]$ and add gaussian noise with standard deviation at 0, 25, and 50 % of signal amplitude. Please refer to Fig. 5 for examples.

Remark 7.1 There are two reason why we regard constant functions as nonperiodic. On the one hand, the intended application for SW1PerS (Sliding Windows and 1-Persistence Scoring) is to identify genes that are both relevant and exhibit a periodic expression pattern with respect to time. Relevance in this case means that changes in expression level translate into physiological phenomena. The second reason has to do with the philosophy of the proposed method: we quantify periodicity as the prominence of 1-homology classes in the sliding-window point cloud. Since this point cloud for a constant function is only a point, it does not have 1-homology and hence is interpreted as coming from a nonperiodic function.

For the Sliding Windows + 1D \mathbb{F}_p -Persistence computation we let $N = 10$, $L = 2$, and $p = 11$. To address noise, we include a layer of (simple) moving average at the sampled signal level and one iteration of mean shift [8] at the sliding-window point cloud level. For the moving average we fix a window size with seven data points and use a cubic spline of this denoised signal to populate the point cloud. Mean shift on a pointwise centered and normalized point cloud X_S was implemented as follows: given a point $x \in X_S$, we let \bar{x} be the mean of the set

$$\{y \in X_S : 1 - (x \cdot y) < \epsilon\},$$

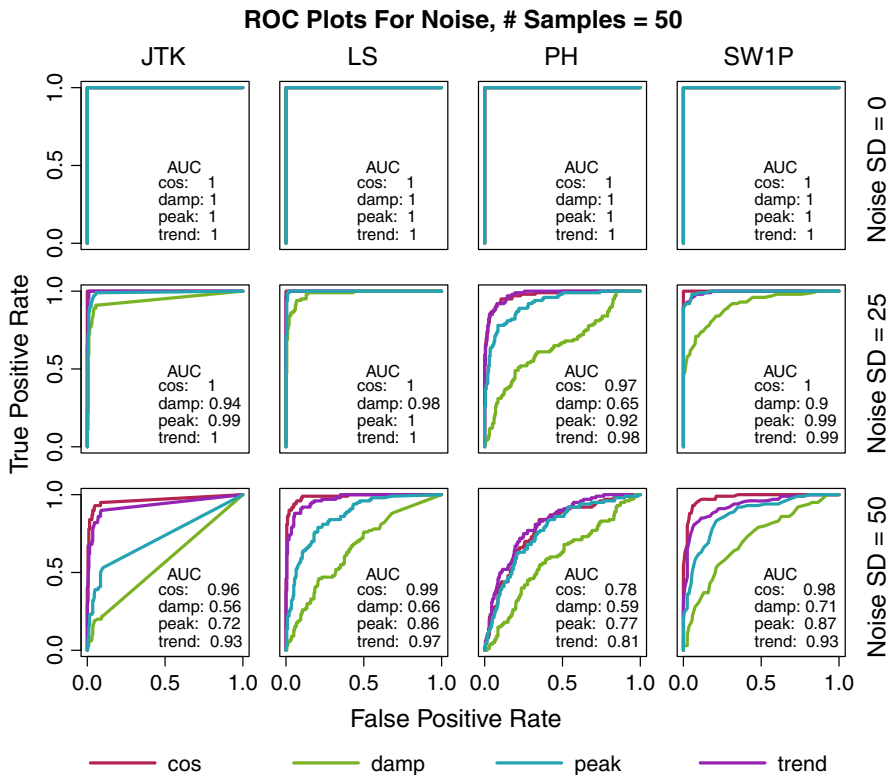


Fig. 6 ROC curves: true positive rate versus false positive rate. We compare the classification success of each algorithm on the synthetic data set using the area under its ROC curves. Curves are colored according to the type of periodic shape, and the area under the curve (AUC) is reported. Please refer to electronic version for colors

where $\epsilon = \cos\left(\frac{\pi}{16}\right)$ and $x \cdot y$ denotes the Euclidean inner product of x and y . In other words, \bar{x} is the mean of the ϵ -neighbors of x if distance is measured by cosine similarity. We obtain the mean-shifted point cloud

$$\bar{X}_S = \left\{ \frac{\bar{x}}{\|\bar{x}\|} : x \in X_S \right\},$$

which we now use for the persistent-homology computation. We report our results in Fig. 6.

The Lomb–Scargle periodogram is considered to be one of the best methods for detecting periodicity, and its ROC curves support this belief. The fact that it is attuned to favoring cosinelike curves makes it very resilient to dampening, trending, and noise. It was thus a great surprise to see that our method performs comparably well in all cases, except for trended cosines and cosines, and that outperforms it for peaked and damped profiles at high noise levels.

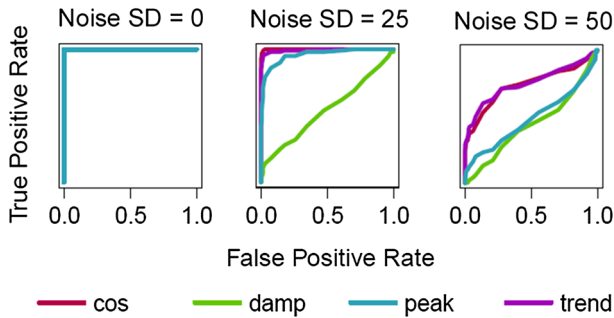


Fig. 7 ROC curves for SWIPerS analysis on raw synthetic data, that is, we do not apply moving average or mean shift. For a comparison on the effect of denoising, please refer to the rightmost column in Fig. 6

A final point we would like to make is that denoising really is a crucial element of the SWIPerS pipeline. We show in Fig. 7 the results of quantifying periodicity on raw synthetic data, i.e., without applying denoising. As one can see, in the absence of preprocessing, the results degrade considerably.

8 Final Remarks

In this paper we proved results that describe the structure of persistence diagrams obtained by sliding-window embeddings of time series. The main tools for the analysis were a Fourier series approximation argument and the stability theorem for persistence diagrams. The results we obtained, provide explicit information about how diagrams from sliding-window point clouds depend on the embedding dimension, window size, and field of coefficients. We then presented examples of the effectiveness of our method for quantifying periodicity of time series data. The experimental side of this framework will be explored in more depth in future work.

This paper also presented the first full *theoretical analysis* of the use of persistent homology in finding structure in time series data. Time-delay embeddings as a means to analyze signals is not new; rather, it is a well-established method in dynamical systems and in image analysis. In addition, the use of computational topology methods to find structure in transformed data has already been considered experimentally, notably in [4] and [10]. This paper, however, is the first to provide a theoretical analysis of the dependency of persistence on the embedding dimension and window size.

There are some interesting new aspects of the use of persistence in this method. It provides one of the first examples where persistent **homology** with coefficients other than \mathbb{F}_2 is required. Other notable examples include [4], where coefficients in \mathbb{F}_3 were essential to discovering the embedded Klein bottle, and [9] and [10], where the authors start with a 1D persistent **cohomology** class mod \mathbb{F}_p and lift it to an integer 1D class to obtain a map to the circle. They do this by choosing p such that the relevant homomorphism in the Bockstein long exact sequence is surjective. Their approach to real data is to choose a prime p at random and evaluate whether $H^2(X, \mathbb{Z})$ has p -torsion. If it does, they then choose another prime. By contrast, we have established

exactly how to determine which primes could be problematic, which allows us to avoid them in advance.

It was highlighted in Remark 4.4 that maximum persistence, the main feature for periodicity studied in this paper, satisfies $mp(\text{dgm}) = 2d_B(\text{dgm}, \text{dgm}_\Delta)$. This is in fact part of a bigger picture. Indeed, the q -Wasserstein distance between two persistence diagrams dgm_1 and dgm_2 is defined by

$$W_q(\text{dgm}_1, \text{dgm}_2) = \min_{\phi} \left(\sum_{\mathbf{x} \in \text{dgm}_1} \|\mathbf{x} - \phi(\mathbf{x})\|_{\infty}^q \right)^{\frac{1}{q}},$$

where $\phi : \text{dgm}_1 \rightarrow \text{dgm}_2$ is a matching of dgm_1 with dgm_2 . As with the bottleneck distance (Remark 4.4), one can show that

$$W_q(\text{dgm}, \text{dgm}_\Delta) = \frac{1}{2} \left(\sum_{(x,y) \in \text{dgm}} (y-x)^q \right)^{\frac{1}{q}},$$

and since $W_q \rightarrow d_B$ as $q \rightarrow \infty$, $2W_q(\text{dgm}, \text{dgm}_\Delta)$ can be regarded as a smoother version of $mp(\text{dgm})$. When dgm comes from a sliding-window point cloud, $2W_q(\text{dgm}, \text{dgm}_\Delta)$ can be interpreted as a sequence of signatures, or features, for periodicity and other phenomena at the signal level. Here the parameter q serves as the level of smoothing, and as it gets larger, the emphasis in what $W_q(\text{dgm}, \text{dgm}_\Delta)$ measures shifts from topological noise and fine attributes to large topological events.

The ring of algebraic functions on persistence diagrams, as a source of features for machine learning purposes, was recently studied by [1]. We believe these and other signatures, such as $W_q(\text{dgm}, \text{dgm}_\Delta)$, should uncover nontrivial signal properties captured by their sliding-window point clouds. We devoted this paper to exploring the use of $mp(\text{dgm})$, but we hope that in future work the list of useful features from persistence diagrams on sliding-window point clouds can be extended.

We also mention that Sect. 6.3 is the first explicit computation of the persistence diagram of a parameterized space. The method of Fourier approximation presented here is one of the first in a much-needed toolbox for explicit computations of persistence diagrams.

Our final comment is to point out that the fact that the size of the sliding window should match the period searched for was not obvious in advance. Knowing this provides powerful information on sampling density to scientists planning an experiment that looks for periodic data and lays the groundwork for the use of SW1PerS as a *filter* for time series data.

In future work we plan to establish our conjecture that $mp(\text{dgm})$ is maximized by our choice of window size, and the main ingredient will be strengthening the lower bound presented in Theorem 6.8. We also plan to establish the filtering properties of SW1PerS and apply it to a variety of data, including biological data like those from gene expression and physiology, astronomical data, and weather. Finally, we plan to extend these methods using other tools from topological data analysis to find structure and features in time series.

Acknowledgments Both authors were supported in part by DARPA under Grants D12AP00001 and D12AP00025-002 and by the AFOSR under Grant FA9550-10-1-0436.

References

1. A. Adcock, E. Carlsson and G. Carlsson, The Ring of Algebraic Functions on Persistence Bar Codes, Preprint <http://comptop.stanford.edu/u/preprints/multitwo>, 2012
2. A. J. Blumberg, I. Gal, M. A. Mandell and M. Pancia, Persistent homology for metric measure spaces, and robust statistics for hypothesis testing and confidence intervals, arXiv preprint <http://arxiv.org/pdf/1206.4581>, 2012
3. G. Carlsson, Topology and Data, Bulletin of the American Mathematical Society, vol 46(2), pp. 255–308, 2009.
4. G. Carlsson, T. Ishkhanov, V. de Silva and A. Zomorodian, On the local behavior of spaces of natural images, International Journal of Computer Vision, vol 7(1), pp. 1–12, 2008.
5. F. Chazal, D. Cohen-Steiner, M. Glisse, L. J. Guibas, and S. Y. Oudot, Proximity of persistence modules and their diagrams, In SCG, pp. 237–246, 2009.
6. D. Cohen-Steiner, H. Edelsbrunner and J. Harer, Stability of persistence diagrams, Discrete and Computational Geometry, vol 37(1), pp. 103–120, 2007.
7. D. Cohen-Steiner, H. Edelsbrunner, J. Harer and Y. Mileyko, Lipschitz Functions Have L^p -Stable Persistence, Foundations of Computational Mathematics, vol 10(2), pp. 127–139, 2010.
8. D. Comaniciu and P. Meer, Mean shift: A robust approach toward feature space analysis, Pattern Analysis and Machine Intelligence, vol 24(5), pp. 603–619, 2002.
9. V. de Silva, D. Morozov and M. Vejdemo-Johansson, Persistent Cohomology and Circular Coordinates, Discrete & Computational Geometry, vol 45(4), pp. 737–759, 2011.
10. V. de Silva, P. Skraba and M. Vejdemo-Johansson, Topological Analysis of Recurrent Systems, Workshop on Algebraic Topology and Machine Learning, NIPS 2012, Preprint available at url: <http://sites.google.com/site/nips2012topology/contributed-talks>
11. A. Deckard, R. Analfi, D. Orlando, J. Hogenesch, S. Haase and J. Harer, Design and Analysis of Large-Scale Biological Rhythm Studies: A Comparison of Algorithms for Detecting Periodic Signals in Biological Data, Bioinformatics, btt541v1-btt541, 2013.
12. H. Edelsbrunner and J. Harer Computational Topology, an Introduction, American Mathematical Society, (2010) (241 pages).
13. E. F. Glynn, J. Chen and A. Mushegian, Detecting periodic patterns in unevenly spaced gene expression time series using Lomb-Scargle periodograms, Bioinformatics, vol 22(3), pp. 310–316, 2006.
14. A. Hatcher Algebraic Topology. Cambridge Univ. Press, England, 2002.
15. M. E. Hughes, J. B. Hogenesch and K. Kornacker, JTK-CYCLE: An Efficient Nonparametric Algorithm for Detecting Rhythmic Components in Genome-Scale Data Sets, Journal of Biological Rhythms, vol 25(372), pp. 372–380, 2010.
16. H. Kantz and T. Schreiber, Nonlinear Time Series Analysis, Cambridge University Press, 2003.
17. H. S. Kim, R. Eykholt and J. D. Salas, Nonlinear dynamics, delay times, and embedding windows, Physica D: Nonlinear Phenomena, vol 127(1), pp. 48–60, 1999.
18. N. R. Lomb, Least-squares frequency analysis of unequally spaced data, Astrophysics and Space Science, vol 39, pp. 447–462, 1976.
19. Y. Mileyko, S. Mukherjee, and J. Harer, Probability measures on the space of persistence diagrams, Inverse Problems, 27(12), p.p. 124007, 2011.
20. K. Mischaikow and V. Nanda, Morse Theory for Filtrations and Efficient Computation of Persistent Homology, To appear on Discrete and Computational Geometry, 2013.
21. J. R. Munkres Elements of Algebraic Topology. Addison-Wesley, Redwood City, California, 1984.
22. M. A. Pinsky, Introduction to Fourier Analysis and Wavelets, The Brooks/Cole Series in Advanced Mathematics, USA, 2003.
23. J. A. Perea, A. Deckard, S. B. Haase and J. Harer, SW1PerS: Sliding Windows and 1-Persistence Scoring; Discovering Periodicity in Gene Expression Time Series Data, preprint (2013).
24. J. D. Scargle, Studies in astronomical time series analysis. II-Statistical aspects of spectral analysis of unevenly spaced data, Astrophysical Journal, vol 263, pp. 835–853, 1982.
25. C. J. Stam, Nonlinear dynamical analysis of EEG and MEG: Review of an emerging field, Clinical Neurophysiology, 116, pp. 2266–2301, 2005.

26. N. Hundewale, The application of methods of nonlinear dynamics for ECG in Normal Sinus Rythm, *Int. J. of Computer Science*, 9, pp. 458–467, 2012.
27. C. E. Shannon, Communication in the presence of noise, *Proc. Inst. Radio Eng.*, vol. 37, no. 1, pp. 10–21, 1949.
28. F. Takens, Detecting strange attractors in turbulence. in D. A. Rand and L. -S. Young. *Dynamical Systems and Turbulence*, Lecture Notes in Mathematics, vol. 898. Springer-Verlag. pp. 366–381.
29. A. Tausz, M. Vejdemo-Johansson and H. Adams, JavaPlex: A research software package for persistent (co)homology, 2011, Software available at url: <http://code.google.com/p/javaplex>
30. A. Zomorodian and G. Carlsson, Computing Persistent Homology, *Discrete & Computational Geometry*, vol 33(2), pp. 249–274, 2005.

Copyright of Foundations of Computational Mathematics is the property of Springer Science & Business Media B.V. and its content may not be copied or emailed to multiple sites or posted to a listserv without the copyright holder's express written permission. However, users may print, download, or email articles for individual use.